



1 Late Eocene to early Oligocene productivity events in the proto- 2 Southern Ocean as drivers of global cooling and Antarctica 3 glaciation

4 Gabrielle Rodrigues de Faria^{1, 2}, David Lazarus¹, Johan Renaudie¹, Jessica Stammerer³, Volkan
5 Özen^{1, 2}, Ulrich Struck^{1, 2}

6 ¹Museum für Naturkunde, Leibniz Institute for Evolution and Biodiversity Science, Invalidenstraße, 43, Berlin, 10115,
7 Germany

8 ²Freie Universität Berlin, Institute for Geological Sciences, Malteserstraße 74-100, Berlin, 12249, Germany

9 ³GFZ German Research Centre for Geosciences, Telegrafenberg, Potsdam, 14473, Germany

10 *Correspondence to:* Gabrielle Rodrigues de Faria (gabrielle.faria@mfn.berlin)

11 **Abstract.** The Eocene-Oligocene transition (ca 40-33 Ma) marks a transformation from an ice free to an ice-house
12 climate mode that is well recorded by oxygen stable isotopes and sea surface temperature proxies. Opening of the
13 Southern Ocean gateways and decline in atmospheric carbon dioxide have been hypothesised as possible triggers of the
14 major climate shift during the Cenozoic. However, the identification of the driving mechanisms remains controversial
15 and it depends on a better understanding of how the different environmental changes correlate to each other. In this
16 study, we investigate the spatio-temporal variation in export productivity using biogenic Ba (bio-Ba) from different
17 Ocean Drilling Program (ODP) Sites in the Southern Ocean, focusing on possible mechanisms that controlled them as
18 well as correlation of export productivity changes to changes in the global carbon cycle. We document two significant
19 SO region high export productivity late-Eocene events (ca. 37 and 33.5 Ma) that are correlated to pronounced changes
20 in global atmospheric $p\text{CO}_2$. We propose that paleoceanographic changes that followed Southern Ocean gateway
21 openings, along with more variable increases in circulation driven by episodic expansion and decline of the Antarctic
22 ice sheet, drove enhanced SO export production in the late Eocene through basal Oligocene. These factors may have
23 driven the episodic reduction of atmospheric carbon dioxide and contributed to Antarctic glaciation during the Eocene-
24 Oligocene transition.

25 1 Introduction

26 1.1 The late Eocene Events as Precursor to Antarctic Eocene/Oligocene Boundary Glaciation

27 The Eocene-Oligocene transition (EOT, ~ 40-33 Ma) is the most important climatic interval of the Cenozoic era
28 (Kennett, 1977; Miller et al., 2009). This interval involves profound transformations in environmental conditions
29 including the onset of continental-scale Antarctica glaciation at the Eocene-Oligocene boundary (Shackleton & Kennett,
30 1975; Zachos et al., 1996; Coxall et al., 2005), sea-level fall (Houben et al., 2012) and global cooling (Prothero and
31 Berggren, 1992; Liu et al., 2009; Bohaty et al., 2012; Hutchinson et al., 2021) as evidenced by a global shift in oxygen
32 isotope records from biogenic calcium carbonate (>1‰; Zachos et al. 2001; Coxall et al. 2005; Bohaty et al., 2012;
33 Westerhold et al., 2020). A positive deep-sea carbon isotope excursion of up to 1‰ (Zachos et al., 2001, Coxall et al.,
34 2005; Coxall and Wilson, 2011; Westerhold et al., 2020) and a change from a shallow (~3.5 km) to a deeper (~4.5 km)
35 calcite compensation depth (CCD) (Coxall et al., 2005; Rea and Lyle, 2005; Pälike et al., 2012; Dutkiewicz and Müller,
36 2021; Taylor et al., 2023) have also been observed and indicate that the carbon cycle played an important role in the



37 changes observed during the transition, although the mechanisms that caused the carbon cycle perturbation are still
38 unsolved.

39 Carbon cycling acts through a variety of feedback mechanisms. Even though it is well recognized that changes in
40 atmospheric carbon dioxide (CO₂) impact the Earth's climate because of its large effect on temperature (Arrhenius,
41 1896; IPCC, 2021), the mechanisms controlling CO₂ over long timescales are still a matter of debate. The carbon cycle
42 perturbation at the EOT provides an opportunity to understand climate-carbon cycle feedback (Zachos and Kump,
43 2005). The mechanisms proposed to explain such perturbations are processes operating gradually over long timescales,
44 and thus likely to have had their origins around the middle to late Eocene.

45 Preceding the abrupt change at the E/O boundary, the late Eocene was a period of gradual cooling and progressive CO₂
46 decrease (Lauretano et al., 2021). The events associated with this time period may have had substantial importance to
47 trigger the major climatic shift at the E/O boundary. The potential main drivers for the initiation of this global cooling
48 and ice build-up in Antarctica are actively debated. Declining global atmospheric carbon dioxide concentrations, and the
49 opening of Southern Hemisphere oceanic gateways, namely the Drake Passage (DP) and the Tasmanian Gateway (TG),
50 are the two main proposed hypotheses to explain this transition (Coxall and Pearson, 2007; DeConto et al. 2008). The
51 decline of carbon dioxide levels are an important factor in driving cooler temperatures, and have been suggested as the
52 crucial factor in the EOT cooling and subsequent build-up of continental glaciers on Antarctica (DeConto and Pollard,
53 2003; Huber and Nof, 2006; Pagani et al., 2011). Atmospheric CO₂ partial pressure (*p*CO₂) decline has observational
54 support during the E/O boundary by independent proxies, showing levels falling below 800 ppm (Pearson, 2009; Pagani
55 et al. 2011; Zhang et al., 2013; Anagnostou et al. 2016), although data is sparse and thus details of the magnitude and
56 timing are still unclear. Atmospheric *p*CO₂ has shown to decline through the Eocene, from ca 2000 ppm in the Middle
57 Eocene (Bijl et al., 2010) to ca. 1000 ppm in the latest Eocene (Pearson et al., 2009). While *p*CO₂ reconstructions have
58 advanced, there is marked variation between different proxies and the absence of tighter constraints on causative
59 mechanisms requires further investigation of the carbon-climate interactions.

60 The tectonic opening of the Southern Ocean gateways is considered a trigger mechanism of the climatic shift because it
61 allows the initiation of the Antarctic Circumpolar Current (ACC) (Kennett, 1977; Barker, 2001; Scher and Martin,
62 2006; Toumoulin et al. 2020). This intense eastward flowing current is proposed in this hypothesis to impact the
63 regional and global climate by preventing tropical heat of low latitudes from reaching Antarctica, promoting the thermal
64 isolation of Antarctica (Kennett and Shackleton, 1976). Numerous ocean circulation model studies of this hypothesis
65 have yielded conflicting results (De Conto & Pollard, 2003; Goldner et al., 2014; Inglis et al., 2015; Ladant et al., 2014;
66 Mikolajewicz et al., 1993; Najjar et al., 2002; Sijp et al., 2009) but most of these earlier works were limited by
67 unrealistic boundary conditions or other issues (Toumoulin et al., 2020, Hutchinson et al., 2021). Recent modelling
68 circulation studies (e.g. Toumoulin et al., 2020; Sauermilch, et al. 2021) demonstrate the importance of the Southern
69 gateway openings and the proto-ACC on ocean cooling in the Southern Hemisphere. Additionally, glaciation has itself a
70 strong influence both on the circulation of the Southern Ocean and on global climate, via increased albedo, colder
71 temperatures and increased latitudinal temperature gradients, and stronger zonal winds (Goldner et al., 2014). There is
72 increasing evidence for at least partial, if transient Antarctic continental glaciation within the late Eocene (Scher and
73 Martin, 2014), and thus this also needs to be considered in understanding how climate and ocean change developed
74 within this period.

75 Moreover, the ACC is associated with the development of fronts that contribute to upwelling-induced biological
76 productivity (Chapman et al., 2020). Considering that the changes in the Southern Ocean circulation have the potential



77 to affect export productivity and the role of export productivity in removing $p\text{CO}_2$ from the ocean-atmosphere system,
78 the 'CO₂' hypothesis and the 'tectonic' hypothesis may be linked, via the influence that gateways may have had on
79 Southern Ocean circulation, increasing export productivity enough to affect global $p\text{CO}_2$. Therefore, evaluating export
80 productivity patterns in the Southern Ocean across the Eocene-Oligocene and its relationship with circulation and
81 decline of atmospheric carbon dioxide during this time period provide important information about the climate feedback
82 in this prominent climatic transition.

83 Many studies have shown variations in biological productivity at this time interval (Diester-Haass, 1995; Diester-Haass
84 and Zahn, 1996; 2001, Salamy and Zachos, 1999; Diester-Haass and Zachos, 2003; Schumacher and Lazarus, 2004;
85 Anderson and Delaney, 2005; Villa et al., 2014), pointing towards a productivity increase associated with ocean
86 circulation changes that increased surface water nutrient availability (Diester-Haass 1992; Zachos et al 1996). However,
87 existing studies have mostly focused on a single site, whose paleoceanographic history may reflect local rather than
88 regional developments. A much broader spatial investigation is particularly important for understanding the influence of
89 large-scale ocean circulation on this process. Moreover, the timing of productivity changes differs among the studies
90 and different proxies, limiting our understanding of cause-and-effect relationship, therefore, highlighting the importance
91 of constrained age models and consistent paleoproductivity proxy.

92 Here, we reconstruct the changes in export productivity across the late Eocene and early Oligocene, and evaluate how
93 the changes observed may be linked to ocean circulation changes and contributed to the climate changes observed at
94 this interval. We utilize biogenic barium (*bio*-Ba) accumulation rates to measure marine export productivity. *Bio*-Ba is
95 defined as the fraction of total barium that not associated with terrigenous sources, sometimes referred as *excess*-Ba
96 (Dymond et al., 1992), it has been applied in several studies in the Paleogene (eg. Nielsen et al., 2003; Anderson and
97 Delaney, 2005; Faul and Delaney, 2010), and is considered a relatively reliable proxy to estimate changes in
98 paleoproductivity in the Southern Ocean. Newly generated carbon and oxygen stable isotope records from the same
99 samples of our *bio*-Ba data constrain the question of the causative mechanisms for the climatic shift at the EOT. We
100 compare our export productivity proxy results to indicators of ocean circulation change, including how these changes
101 correspond with gateways opening, paleoceanographic changes, ice sheet history, and their influence on marine
102 biological productivity. We also compare our productivity records to proxies for the global carbon cycle, specifically
103 $p\text{CO}_2$ and $\delta^{13}\text{C}$ of benthic deep sea foraminifera. Advancing our understanding of the cause of this event is crucial in
104 identifying the mechanisms governing global climate change.

105 Although much of our understanding of the Eocene-Oligocene transition has been achieved through modelling studies
106 as they provide means to compare several possible scenarios, this paper focuses on proxy evidence of the changes that
107 occurred in this time interval. Our multiproxy approach and wide coverage allow us to test the hypotheses:

108 H1: Changes in ocean circulation patterns that took place during the late Eocene and early Oligocene (eg. development
109 of ACC and strengthening of AMOC) contributed to the increase in biological productivity in the Southern Ocean.

110 H2: The magnitude of the export productivity increase during a time period that preceded the EOT may have been an
111 important contribution to the drawdown of $p\text{CO}_2$.

112 First, we investigate the export productivity changes across the late Eocene to early Oligocene in two different regions
113 in the Southern Ocean. Then we compare our results to the paleo-circulation changes that occurred at the same time
114 period. We conclude by summarising the implications of the changes in ocean circulation and the possible climate
115 driving mechanisms that led to the cooling of Earth.

116 1.2. Paleoceanographic Setting



117 The Southern Ocean (SO) today is an important part of the global ocean circulation and climate system, interconnecting
118 the Atlantic, Pacific and Indian Ocean basins, providing and thus inter-basin exchange of ocean properties and heat.
119 There are strong latitudinal gradients and seasonal changes in ocean properties which affect surface water and export
120 productivity, and thus this region's role in global carbon capture and sequestration. Low light levels and, in higher
121 latitudes, extensive sea ice limit productivity during the winter months. Deep surface mixed layers over the large areas
122 of the Southern Ocean, beyond the shallow stratification effects of meltwater near the sea ice edge, also tend to limit
123 productivity in spring through fall as plankton is mixed below critical thresholds of light availability. The relationship
124 between mixed layer thickness and productivity however is complex (Nelson and Smith, 1991; Li et al. 2021). Southern
125 Ocean productivity is thus concentrated near the Antarctic Circumpolar Current (ACC), the dominant current in the
126 region. This current is the longest and strongest ocean current on Earth. This complex circulation system is driven
127 mainly by westerly winds, resulting in Ekman transport and favouring deep water upwelling. This flow pattern is
128 possible in the absence of land barriers and is balanced by bottom topography friction (Rintoul et al., 2001; Carter et al.,
129 2008), while the strength of the current is driven by the strength and location of the westerly winds, and thus, among
130 other factors, the global latitudinal thermal gradient. The ACC is a key component of the 'ocean conveyor belt', playing
131 a role in the global transport of heat (Katz, et al. 2011). Moreover, this circumpolar current influences the strength of
132 meridional overturning circulation and several authors have proposed that this current is one of the main drivers of the
133 Atlantic meridional overturning circulation (AMOC) (Toggweiler and Samuels, 1995; Toggweiler and Bjornsson, 2000;
134 Scher and Martin, 2006, Kuhlbrodt et al., 2007, Scher et al., 2015, Sarkar et al., 2019).

135 The ACC is structured of multiple hydrological fronts, associated with specific water mass properties such as
136 temperature and salinity (Sokolov and Rintoul, 2009). Orsi et al., 1995 were the first to propose the traditional view of
137 Southern Ocean fronts. It consists of the Subantarctic Front (SAF), the Antarctic Polar Front (APF) and the Southern
138 ACC Front (SACCF). Besides these main fronts, a Subtropical Frontal Zone (STFZ) can be found north of the ACC
139 (Orsi et al., 1995; Palter et al. 2013; Chapman 2020). This frontal structure is fundamental to different processes that
140 occur in the region, such as the distribution of important nutrients through the exchange between deep and surface
141 ocean, and the exchange of tracers (Palter et al., 2013). Upwelling of Circumpolar Deep Water (CDW) brings nutrient-
142 rich waters to the surface towards the Polar Front Zone (PFZ) where Antarctic Surface Waters (AASW) sink to form
143 Antarctic Intermediate Water (AAIW), thereafter it extends into the Subantarctic Zone (SAZ) (Sarmiento et al., 2004)
144 (Figure 1).

145 Wind-driven upwelling, that occurs within the Southern Ocean fronts, enhance biological productivity in these regions
146 (De Baar et al., 1995; Moore et al., 1999). More recently, upwelling related to ACC bathymetry has been found as an
147 important mechanism for establishing phytoplankton blooms in the SO (Sokolov and Rintoul, 2007). This complex
148 structure involving ACC fronts, westerlies and the bottom topography, makes the Southern Ocean a highly productive
149 region. Iron remobilisation has also been shown to occur due to latitudinal variations of the ACC (Kim et al., 2009),
150 hence inducing a massive increase in productivity.

151 During the Cenozoic, the ACC structure began to develop with the opening of the pathways between South America and
152 Antarctica and the following formation of the Drake Passage (DP) and, also between Australia and Antarctica that
153 allows the Tasmanian Gateway (TG) opening. Removing these geographic barriers permitted the gradual development
154 of circumpolar flow (Toggweiler and Bjornsson, 2000). The TG opening to intermediate and deep waters occurred in
155 the late Eocene, ca 35.5 Ma (Stickley et al., 2004). Tectonic reconstructions for the Drake Passage timing opening
156 remain controversial, ranging from the late Eocene (ca 41 Ma; Scher and Martin, 2004, 2006) to the early Miocene (ca



157 23 Ma, Barker 2001). Even if the timing of the deepening of the Drake Passage is less well constrained, a “proto-ACC”
158 has been proposed as an earlier expression of the ACC and it is defined as a shallow-depth circumpolar current (Scher
159 et al., 2015, Sarkar, et al., 2019). Cramer et al. 2009 suggested that “proto-ACC” would have played an important role
160 in the ocean circulation changes that occurred in the Eocene.

161 Many climate model studies have contributed with insights into the ocean structure and circulation of the late Eocene
162 (e.g. Huber et al. 2004, Huber & Not 2006, Sijp et al., 2011, Sijp et al., 2016, Elsworth et al., 2017, Baasten et al, 2020,
163 Toumoulin, et al., 2020). Although some of these experiments have shown that opening of gateways was not sufficient
164 to have caused the global cooling recorded by proxies (DeConto & Pollard, 2003, Huber et al. 2004, Huber & Not 2006,
165 Sijp et al., 2011, Baasten et al., 2020), they acknowledge that the circulation patterns have changed during the Eocene.
166 A recent model circulation experiment has demonstrated the impact of the DP opening and its effects on ocean structure
167 and dynamics even for shallow depths (Toumoulin et al., 2020).

168 The organisation of Southern Ocean proto-oceanic fronts may have occurred during the Eocene and formed poleward
169 (proto-PF: $\sim 70\text{--}60^\circ\text{S}$; proto-STF: $65\text{--}50^\circ\text{S}$) of their present-day positions, progressing to lower latitudes during the
170 Oligocene and Miocene (Lazarus and Caulet, 1994; Nelson and Cooke, 2001; Cooke et al, 2002). This frontal zone
171 migration likely played a role in major changes at that time period, including higher ocean productivity.

172 Evidence of significant events during the late Eocene highlights the importance of this period that preceded the
173 permanent glaciation in Antarctica. Increasingly heavy global benthic oxygen isotope values in the late Eocene, at ca 37
174 Ma have been interpreted to reflect pre-EOT glaciation and cooling, this episode is referenced as PrOM event
175 (Priabonian Oxygen isotope Maximum, Scher et al., 2014). Additional evidence for a prominent cooling episode has
176 been found during this time period (Anderson et al., 2011, Douglas et al., 2014). Despite uncertainties about the nature
177 and extent of the earliest ice in Antarctica, these changes imply that paleogeographic reconfiguration has affected the
178 late Eocene Antarctic climate. It is clear that some combined processes favoured the development of permanent
179 glaciation in Antarctica.

180 Given the importance of changes during the Eocene-Oligocene time interval, especially the ACC development and its
181 frontal structure to the climate system and ecosystems, it is crucial to investigate the timing and magnitude of late
182 Eocene paleoceanographic changes in the Southern Ocean, and equally important to expand our understanding of the
183 implications of such changes on paleoproductivity and how these mechanisms are linked to a changing climate.

184 **2 Materials and Methods**

185 **2.1 Site Descriptions**

186 We investigated sediment samples from 3 Ocean Drilling Program (ODP) Sites in the Southern Ocean (Table 1). ODP
187 Leg 177 Site 1090 on the southern flank of the Agulhas Ridge in the Southern Atlantic Ocean ($42^\circ 54.8'\text{S}$, $8^\circ 53.9'\text{E}$,
188 water depth 3,702m), ODP Leg 133 Site 689 on Maud Rise in the Southern Atlantic Ocean ($64^\circ 31'\text{S}$, $3^\circ 6'\text{E}$, water
189 depth 2,253m) and ODP Leg 120 Site 748 on Kerguelen Plateau in the Southern Indian Ocean ($58^\circ 26.45'\text{S}$, $78^\circ 58.89'\text{E}$,
190 water depth 1,290.9m). We selected samples from the middle Eocene through the E-O boundary, depending on the
191 sample availability.

192 Currently, the sites studied are located in the Southern Ocean through the ACC. Sites 689 and 748 are located in the
193 south of the Polar Front zone (PFZ) and Site 1090 in the Subantarctic zone, between the Subtropical front (STF) and the
194 Subantarctic Front (SAF) (Figure 1). Across the Eocene-Oligocene transition, the sites were shallower (Table 1). Sites



195 689 and 748 locations were similar to today and site 1090 was as much as 5° farther to the south (Gersonde et al., 1999)
 196 (Table 1).

197 The major lithology from the lower Eocene to the upper Oligocene at the Maud Rise is composed of calcareous and
 198 silicious oozes (Barker et al., 1988). Kerguelen Plateau site is composed mainly of nannofossil ooze and chert (Barron
 199 et al., 1989). Agulhas Ridge is predominantly composed of diatoms and nannofossil ooze, with CaCO₃ wt% highly
 200 variable, ranging from non-detectable to 69% of sediment throughout the study interval. (Gersonde et al., 1999) with
 201 rare occurrences and barren intervals of planktic and benthic foraminifera making it difficult to establish stable isotope
 202 records on this site.

203 **Table 1.** Position of the ODP Sites studied in the present-day and in the late-Eocene (~ 37 Ma). Paleocoordinates
 204 calculated based on Seton et al. (2012) rotation model.

Site	Geographic Setting	Latitude	Longitude	Water depth (m)	Paleodepths (m)	Paleo-latitude	Paleo-longitude
1090	Agulhas Ridge	42°54.8'S	8°53.9'E	3 702	ca. 3,000-3,300 (Pusz et al. 2011)	ca 47°33'S	ca 1°46.8' E
689	Maud Rise	64°31'S	3°6'E	2 253	ca. 1500 (Diester-Haass and Zahn, 1996)	ca 64°19.2'S	ca 2°43.2' E
748	Kerguelen Plateau	58°26.45'S	78°58.89'E	1 290.9	ca. 1200 (Wright et al., 2018)	ca 56°48.6'S	ca 75°36' E

205 2.2 Age Models, Linear Sedimentation Rates

206 Revised age models for the ODP Site 1090, ODP Site 689 and ODP Site 748 in this study were based on all
 207 magnetostratigraphic and biostratigraphic data available on the Neptune database via NSB system (Renaudie et al.,
 208 2020) (Figures S1-S4). All ages in our study are given in the Gradstein et al. (2012) GPTS scale, or have been remapped
 209 to this scale from prior studies.

210 ODP Site 177 1090 has an age model constructed from shipboard magnetostratigraphic data “U-channel”, the records fit
 211 the geomagnetic polarity timescale (GPTS) (Channell et al., 2003). Nannofossil biostratigraphy has confirmed the
 212 Chron ages (Marino and Flores, 2002), as well as foraminiferal biostratigraphy (Galeotti et al. 2002), strontium isotopes
 213 (Channell et al., 2003) and oxygen and carbon isotope data from benthic foraminifera (Zachos et al., 2001, Billups et
 214 al., 2002). This integration of several age indicators and their consistency makes this a robust and very well constrained
 215 age model.

216 Magnetostratigraphic data for ODP 113 Site 689 is partially reinterpreted from the measurements originally made by
 217 Spiess, 1990. A new high-resolution study of Eocene-Oligocene “U-channel” samples from this site presents high
 218 correlation with the GPTS (Florindo and Roberts, 2005). Ocean calcareous nannofossil datums (Wei and Wise, 1992;
 219 Wei, 1992, Persico and Villa, 2002, 2004), planktonic foraminiferal datums (Kennett and Sott, 1990; Thomas, 1990;
 220 Berggren et al., 1995) and Argon-argon (⁴⁰Ar/³⁹Ar) dating (Glass et al., 1986; Vonhof et al., 2000) is used to re-calibrate
 221 ages for this site.

222 A high-resolution magnetostratigraphic study from ODP Site 748B was carried out by Roberts et al. 2003 in continuous
 223 “U-channel” samples, revising the shipboard analysis from Inokuchi and Heider, 1992. Calcareous nannofossils



225 biostratigraphy (Aubry 1992), planktonic foraminiferal biostratigraphic datums (Berggren et al., 1995), diatom datums
226 (Baldauf and Barron, 1991, Roberts et al., 2003) and strontium isotopes ages (Zachos et al., 1999; Roberts et al., 2003)
227 were re-evaluated for a better age model.

228 Accumulation rate fluxes are obtained by calculating the product of linear sedimentation rates (LSR) and shipboard
229 measured dry bulk densities (DBD), thus a robust age model is crucial for this calculation because it determines the
230 linear sedimentation rates. We present data using a straightforward LSR calculation between age-depth control points
231 based on magnetostratigraphic data, stable isotopes and biostratigraphic data. Mass accumulation rates (MARs, mol cm⁻²
232 kyr⁻¹) were calculated using LSR based on the above age models multiplied by DBD.

233 Since bio-Ba AR is a direct function of LSR, it is essential to evaluate any possible influence. Figure S5 shows a
234 comparison of linear sedimentation rates and bio-Ba AR. This comparison showed a high amplitude peak at ODP Site
235 1090, with LSR of 4.11 cm kyr⁻¹ at the late Eocene, this high rate is based on a very constrained model. The LSRs for
236 ODP Site 689 varies from 0.1 cm kyr⁻¹ during early Oligocene to up to 1.3 cm kyr⁻¹ in the late Eocene, whereas ODP
237 Site 748 has more uniform values during late Eocene. Small adjustments to LSRs may result in large changes in MARs,
238 emphasising the importance of very well constrained age models. The available age data for our sites allow some
239 variation in the placement of the line of correlation, and thus the precise timing and magnitude of sedimentation rate
240 changes on the scale of ± ca.5 m.y. are not well constrained, patterns and calculated values over longer time scales are
241 thought to be robust.

242 **2.3 Stable Isotope Analyses**

243 Stable isotopes of carbon and oxygen were measured both on the bulk fine fraction (<45µm) and benthic foraminifera.
244 Bulk sediments were oven-dried and washed through different sieve sizes (125 and 45µm). Smear slides observations
245 indicate that the main carbonate composition of the fine fraction is coccoliths, therefore stable isotopic compositions of
246 bulk fine fraction (<45 µm) reflect primary nannofossil isotope signals. Contamination by non-coccolith carbonate such
247 as fragments of foraminifera shells is minimal (Figure S5). Fifteen to twenty tests of benthic foraminifera (*Cibicidoides*
248 spp.) were picked from the >125-µm-size fraction. Foraminiferal tests were ultrasonically cleaned using ethanol and
249 oven-dried. Stable isotopic analyses were carried out at the Stable Isotope Laboratory of the Museum für Naturkunde
250 (Berlin, Germany) on a Thermo Isotope Ratio Mass Spectrometer. All values are reported in the δ-notation in parts per
251 mil (‰) relative to the Vienna Pee Dee Belemnite (VPDB). In this study, we applied an adjustment of +0.64‰
252 (Shackleton and Opdyke, 1973; Shackleton et al., 1984) to all δ¹⁸O values of the benthic foraminifera *Cibicidoides* to
253 account for disequilibrium effects.

254 **2.4 Barium Analyses and Biogenic Barium as a Paleoproductivity Proxy**

255 Barium (Ba) and aluminum (Al) were analysed by ICP OES, performed at the EIMiE Lab at the German Centre for
256 Geosciences (GFZ, Potsdam, Germany) using a 5110 spectrometer (Agilent, USA). The analytical precision and
257 repeatability were generally better than 2% and it is regularly tested by certified reference material and in-house
258 standards. For preparation, 2g of each sample were grounded and dissolved with ultra-pure HCL. Intensity calibration
259 was performed by external calibration using the same batch of solvent to ensure matrix matching. The analytical blank
260 was negligible compared to the sample concentration.

261 Using barium as a paleoproductivity proxy requires some adjustments because other biogenic sources may contribute to
262 the barium content in the sediment. Detrital aluminosilicate may affect the barium signal in Southern Ocean sediments.



263 In order to solve this issue and reveal aluminosilicate contributions, the Biogenic Barium calculation was proposed by
264 Dymond et al., 1992, following Eq (1):

$$265 \text{ Biogenic Barium (Bio Ba)} = (\text{Ba total})_{\text{sample}} - (\text{Ba/Al})_{\text{bulk continental crust}} \times \text{Al}_{\text{sample}} \quad (1)$$

266 This assumes that the aluminum (Al) concentration and the average continental crust abundance are representative of
267 the detrital Ba component. The Ba/Al crust ratio of 0.0075 is the global average value from sedimentary rocks as
268 suggested by Dymond et al. (1992). This value is based on various compilations of elemental abundances in crustal
269 rocks. This normative calculation potentially introduces uncertainty in samples with high and variable detrital barium,
270 but considering that clay assemblages and weathering regimes were relatively constant during the early Paleogene in the
271 Southern Ocean, therefore, the crustal ratio probably did not vary much (Robert et al. 2002).

272 **2.5 Data Compilation**

273 **2.5.1 Neodymium Isotope Data**

274 Neodymium isotopes in seawater reflect the different weathering sources of neodymium that affects each water mass.
275 The isotope values act as conservative elements during ocean mixing. They are therefore a robust water mass tracer, and
276 further are faithfully archived in sediments (Piepgras and Wasserburg, 1982; Martin and Haley, 2000). Their behaviour
277 in seawater and the conservation of the signal in sediments make them a valuable proxy for paleoceanographic studies
278 and past ocean circulation reconstruction. Fossilised fish teeth is commonly used and are considered robust archives to
279 extract Nd isotopic signature because they incorporate and preserve their Nd signature during very early diagenesis
280 (Martin and Scher, 2004), and they can be found in deep-sea sediment samples all over the world and in many geologic
281 time intervals. The Nd signal is given in ϵNd , where ϵNd is the ratio $^{143}\text{Nd}/^{144}\text{Nd}$ of a sample relative to the same of the
282 bulk Earth, in parts per 10,000.

283 In this study, we compiled published Nd isotope data from fossil fish teeth, from the same Ocean Drilling Program
284 (ODP) sites that we investigated in the Southern Ocean (ODP Site 1090 Agulhas Ridge, ODP Site 689 Maud Rise and
285 ODP Site 748 Kerguelen Plateau) and explore the Nd isotope variability to examine the intrusion of waters from the
286 Pacific to the Atlantic sector of the Southern Ocean. We then used these data and our records to explore the evolution of
287 the Southern Ocean circulation and significant circulation changes across the Eocene-Oligocene transition. Sources of
288 Nd isotope data are given in Table S1.

289 **2.5.2 $p\text{CO}_2$ Data**

290 A variety of geological proxies have been applied to reconstruct the partial pressure of atmospheric CO_2 ($p\text{CO}_2$) during
291 the Cenozoic Era (Pearson & Palmer, 2000; Pagani et al., 2005; Beerling & Royer 2011). Given the low sampling
292 density through the critical Eocene-Oligocene interval, we compiled published $p\text{CO}_2$ data from marine and terrestrial
293 proxies that have been identified as reliable for reconstructing $p\text{CO}_2$ in the Cenozoic. The marine geochemical proxies
294 include alkenone-based estimations, carbon and boron isotope ($\delta^{11}\text{B}$) composition of well-preserved planktonic
295 foraminifera calcite. Proxies from the terrestrial reservoir include paleosol carbon and stomatal density. Our
296 atmospheric CO_2 compilation (Table S2) consists to our knowledge all the currently available proxy data on most recent
297 Eocene and Oligocene $p\text{CO}_2$ records. Such compilations are commonly used to estimate past $p\text{CO}_2$, although it is
298 known that there are limitations and variation among them (IPCC, 2021). Zhang et al. (2013) specifically argued that



299 compositing limited, short time interval data from different proxies, and different localities may introduce substantial
300 bias into the resulting fitted curve, and instead generated a 40 My long history of Cenozoic $p\text{CO}_2$ from a single section
301 (Site 925 in the equatorial Atlantic). We consider this study's results to be the best single source of information on the
302 history of atmospheric $p\text{CO}_2$. However, precisely because of the substantial amounts of between proxies and between
303 locality variation, data using a single proxy, from a single site is also potentially not representative of global $p\text{CO}_2$
304 history. We thus use both the single site results of Zhang et al. (2013) and the full, multi-site and multi-proxy
305 compilation (Supplementary material) in evaluating our own study's results.

306 **3 Results**

307 **3.1 Biogenic Barium**

308 Biogenic Barium accumulation rate (bio-Ba AR) records (Figure 2) show a pronounced rise in the late Eocene when the
309 values were up to twice as high as in previous periods for all sites studied. At Kerguelen Plateau ODP Site 748, we also
310 observe a previous and smaller increase around the middle Eocene Climatic Optimum (MECO, ca 40 Ma). At Maud
311 Rise the increase began at ca 38.3 Ma and persisted for around 1.5 Myr. bio-Ba ARs show high value in the Agulhas
312 Ridge at ca 36.8 Ma that is induced by a high sedimentation rate (Figure S5a). Although export productivity was higher
313 (maximum values to about $16.8 \mu\text{mol bio-Ba cm}^{-2} \text{ky}^{-1}$) at Maud Rise compared to the other sites -the Kerguelen Plateau
314 reached maximum values of about $14.3 \mu\text{mol cm}^{-2} \text{ky}^{-1}$ and the Agulhas Ridge site $13.74 \mu\text{mol cm}^{-2} \text{ky}^{-1}$, the records
315 show a high degree of temporal correspondence in the late Eocene peak (ca 36.8 Ma). Bio-Ba values were low at all
316 sites between ca 36 and 34.5 Ma. Between ca 34.5 Ma and ca 33.3 Ma, which includes the EOT interval, bio-Ba AR
317 increased in both sites of the Atlantic Sector, but these increases were not very concurrent between the sites
318 investigated. On the Agulhas Ridge, ODP Site 1090, the rise in bio-Ba (from 7.37 to $20.46 \mu\text{mol cm}^{-2} \text{ky}^{-1}$) is observed
319 in the very latest Eocene (ca 34.3), just before the Oi-1 event. At Maud Rise, ODP Site 689, the increase is not observed
320 until ca 1 Myr after, in the early Oligocene (maximum value $16.25 \mu\text{mol cm}^{-2} \text{ky}^{-1}$ at ca 33.3 Ma). On the Kerguelen
321 Plateau, ODP Site 748, the increase in export productivity registered by bio-Ba during the Oligocene is notably smaller
322 than in the Atlantic sites, with values not higher than the low values observed during the Eocene.

323 Our bio-Ba results are in general concordant with the temporally more limited data obtained by prior studies of
324 Southern Ocean sites (Anderson and Delaney, 2005, Site 1090; Diester-Haass and Faul 2019, Site 689) (Figure 2).
325 However our results for Kerguelen Plateau Site 748 differ from those of Faul and Delaney, 2010 for nearby Site 738,
326 where the latter estimate bio-Ba accumulation rates up to twice those obtained in our study of Site 748. The differences
327 may be due to the different locations of the two sites, Site 738 is located several degrees further south, and in ca 1 km
328 deeper water depth. The bio-Ba proxy is also very sensitive to sedimentation rates, and the differences may be due to
329 the poor age control for Site 738 which in our studied time interval consists only of a few rather scattered
330 biostratigraphic events (Figure S4a), which results in substantially different age models between our study, Faul and
331 Delaney (2010), and other recent studies of this site, e.g. Huber and Quillevere (2005). In these studies the location and
332 extent of hiatuses, and the uniformity of sedimentation rates varies considerably (SOM Figure S4b). The age model for
333 Site 748 by contrast (Figure S3) is very well constrained by coherent biostratigraphic events from multiple groups of
334 microfossils, Sr isotope stratigraphy and paleomagnetic stratigraphy, and we therefore accept the results from Site 748
335 as being more reliable.



336 When the data for individual sites is composited together, the behaviour of the Southern Ocean region can be roughly
337 estimated, even though our geographic coverage (lacking data from the Pacific/New Zealand sector) is incomplete and
338 thus may not be entirely representative of the Southern Ocean as a whole. A lowess curve fit to the composited bio-Ba
339 data shows that the key patterns noted in individual records are retained in the composite signal, and thus that Southern
340 Ocean productivity can be characterised as having had two intervals of high values at around 37 and 34 Ma.

341 **3.2 Oxygen and Carbon Isotopes**

342 Our new oxygen (Figure 3C and E) and carbon (Figure 3D and F) stable isotope data allow us to identify previously
343 noted trends and distinct events during the period studied. Benthic $\delta^{18}\text{O}$ values exhibit an overall increasing trend during
344 the late Eocene indicating the overall decrease of oceanic bottom water temperatures. A sharp increase occurs at the
345 Eocene-Oligocene transition (between 33.9 and 33.3 Ma) in both sites examined. This rapid shift has been observed in
346 several sites in the Southern Ocean (e.g., Muza et al., 1983; Miller et al., 1987; Mackensen and Ehrmann, 1992; Zachos
347 et al., 1996; Billups et al., 2002; Pusz et al., 2011) and it is well established as a global signal (Zachos et al., 2001). It is
348 generally interpreted as a combination of deep ocean water cooling and major ice growth on the Antarctic continent
349 (Zachos et al., 2001). At Site 689, the planktic $\delta^{18}\text{O}$ curve almost mimics the benthic one. The $\delta^{18}\text{O}$ values measured on
350 fine fraction reveal a heavier trend more pronounced at ODP Site 748 (Kerguelen Plateau) compared to ODP Site 689
351 (Maud Rise). During the Eocene, heavier values are observed around 37 Ma in both Atlantic and Indian Sectors of SO.
352 Both benthic and planktic foraminifera $\delta^{13}\text{C}$ records show fluctuations across the period studied, with low values across
353 the Eocene-Oligocene boundary, followed by an increase that accompanied the $\delta^{18}\text{O}$ increase and low values again in
354 the upper Oligocene. The benthic trend is also observed by previous data from the same sites (Mackensen and Ehrmann,
355 2002; Diester-Haass and Zahn, 1996; Bohaty et al., 2003). The fine fraction records show elevated $\delta^{13}\text{C}$ values between
356 Late Eocene to Early Oligocene, followed by a decreasing trend during the Oligocene (from ca 33.2Ma). At Site 748,
357 the fine fraction $\delta^{13}\text{C}$ curve shows less fluctuation than the benthic curves during the middle Late Eocene. A
358 synchronous $\delta^{13}\text{C}$ increase (ca 0.6‰ shift) is observed at 36.5 Ma. Elevated fine fraction $\delta^{13}\text{C}$ values are observed from
359 the late Eocene until the early Oligocene, coherent with previous studies (Bohaty et al., 2003), while the benthic values
360 stay low during the same period (Figure 3D and F).

361 **3.3 $p\text{CO}_2$ Proxies**

362 As noted above, given the complexities and potential biases of compiling data from different proxies and different time
363 intervals, we prefer to use the single site single proxy time series of $p\text{CO}_2$ from Zhang et al. (2013). This data (Figure 4)
364 shows two peaks in the late Eocene, with a maximum for the entire study interval at ca 37 Ma and a smaller peak at ca
365 34.5 Ma, and a rapid drop of over 200 ppm from nearly 1000 to ca 750 ppm in the earliest Oligocene (ca 33.5 Ma).
366 Despite the limitations of multi-proxy, multi-site compilations, the compiled data (Table S2; Figure S7) shows the same
367 basic features, nor does the result appear to be sensitive to the precise choice of data to include in the analysis.

368 **4 Discussion**

369 **4.1 Late Eocene Productivity Event and its Potential Impact**



370 The noticeable bio-Ba AR peak at ~ 36.8 Ma (Figure 2), suggests an important, ca 1 my long event of approximate
371 doubling of export productivity during the late Eocene, preceding the significant cooling and the first formation of large
372 Antarctic ice sheets at the Eocene-Oligocene boundary. The temporal synchronicity among different site locations in the
373 Southern Ocean suggests that the process driving this enhanced export productivity in the late Eocene occurred
374 throughout the Southern Ocean, requiring a mechanism that increased the delivery of nutrients to the surface ocean.

375 Our findings corroborate previous, more limited paleoproductivity studies that indicate an increase in export
376 productivity in the Atlantic Sector of the Southern Ocean during this time period. Anderson and Delaney (2005) found
377 several peaks in productivity indicators at the Agulhas Ridge during the same time interval, and benthic foraminiferal
378 accumulation rates show an increase in paleo-primary productivity on Maud Rise (Diester-Haass & Faul, 2019) (Figure
379 2). A pronounced opal abundance peak is also documented by Diekman et al. (2004) between 37.5 and 33.5 Ma at the
380 ODP Site 1090. The Kerguelen productivity record from Site 744 data shows a substantial peak around 37 Ma and an
381 earlier one near 40 Ma. Our results thus show that the 37 Ma event extended at least as far as the Kerguelen Plateau in
382 the Indian Ocean sector, thus affecting most of the Southern Ocean region.

383 The potential significance of this event for the development of late Eocene global climate depends on the extent to
384 which the enhanced productivity contributed to enhanced carbon sequestration, and the magnitude of sequestration over
385 the ca 1 my interval of enhancement. Our ability to estimate the impact of higher productivity on carbon sequestration is
386 limited, as many of the factors that affect this in the modern ocean are poorly understood for Eocene oceans (export
387 efficiency to the subsurface waters, rates of transport and degradation in the water column and upper sediment layers,
388 organic carbon content of Southern Ocean Eocene pelagic sediments; as well as transport of organic carbon by
389 subsurface water layers in the late Eocene oceans to lower latitude areas of productivity and sequestration). For
390 simplicity we thus use values for the modern Southern Ocean, but conservatively ignore the (in the modern oceans)
391 substantial transport of nutrients in the modern ocean to lower latitudes by Antarctic Intermediate Water (Sarmiento et
392 al., 2004). The purpose of such a calculation is simply estimating if the magnitude of enhanced productivity, could,
393 within the region studied, and over the 1 my interval of the event, at least potentially have sequestered a climatically
394 significant amount of carbon. Using Hayes et al. (2021) data on the composition and flux of seafloor sediments in the
395 Global Ocean, we compute the mean total organic carbon (TOC) exported to deep-sea sediments per cm² per year in the
396 Southern Ocean (SO, area below the polar front and above the Antarctic continent), the Polar Frontal Zone (PFZ, based
397 on Park et al. 2019 coordinates for the subantarctic and polar fronts) and, as a subset of the SO total, just the Atlantic
398 sector of the Southern Ocean. We thus estimate the total amount of organic carbon currently exported to the deep sea
399 per year in these areas. Finally, given the approximate doubling of productivity during the 1 my interval, we compute
400 the amount of excess exported carbon over 1 Myr, and translate it into the corresponding amount of atmospheric CO₂ in
401 ppm (using Clark 1982 equivalency) to roughly estimate the order of magnitude of how much carbon the biological
402 carbon pump could have buried in the sediments of the area of interest. The results (Table 2) suggest that enhanced
403 carbon sequestration in the late Eocene SO, even if restricted only to the Atlantic sector, could have indeed been
404 sufficient to have affected global *p*CO₂ (hypothesis 2 as stated in the introduction). If the enhanced productivity affected
405 most, or all of the circumpolar region, and if indirect carbon sequestration via intermediate water transport also played a
406 role the impact could have been dramatic.

407 **Table 2.** Potential impact of doubling modern Southern Ocean export productivity/carbon sequestration for a 1 my time
408 interval. See text for definitions of areas and calculations.



Region	Area (km ²)	Mean TOC (gC cm ⁻² yr ⁻¹)	Exported carbon (PgC Myr ⁻¹)	Equivalent pCO ₂ (ppm)
Southern Ocean	35 882 985	0.004882	1 751.856	882.5
PFZ	10 290 123	0.004326	445.108	209.0
Atlantic Sector of SO	11 561 803	0.005047	583.518	274.0

409 4.2 Surface Water Changes in Physical Conditions in the Late Eocene

410 The late Eocene is generally accepted as a time interval of gradual cooling of Southern Ocean waters. Indeed,
411 biomarker-based temperature estimates reveal substantial (3-5 °C) high latitude sea surface temperatures (SST) cooling
412 within the late Eocene (Liu et al., 2009, O'Brien et al., 2020). Our fine fraction stable oxygen isotopes confirm this
413 cooling trend following MECO, with a distinct peak at 37 Ma during the Eocene, matching the peak cooling reported by
414 O'Brien et al. (2020). This interval of maximum $\delta^{18}\text{O}$ values occurred during the same interval in which export
415 productivity increased (Figure 2). In this interval the difference in the $\delta^{18}\text{O}$ gradient between benthic foraminifera and
416 fine fraction (nannofossil) carbonate is less pronounced. This increase in similarity can either be caused by a decrease in
417 water column stratification or by enhanced vertical mixing. In other words, either the (temperature) conditions during
418 deposition were identical across larger areas and depths, or water masses were mixed more frequently.

419 This change in export productivity in the late Eocene is coeval with a change towards increasing variability carbon
420 stable isotopes ($\delta^{13}\text{C}$) of benthic foraminifera (Figure 4). Benthic foraminiferal $\delta^{13}\text{C}$ provides a powerful tracer for the
421 reconstruction of bottom water circulation patterns, nonetheless, should be carefully interpreted because the signal can
422 be overprinted by multiple effects such as the global carbon cycle or local dissolved nutrient contents. Comparing our
423 local stable carbon isotope records to a global compilation shows that the local $\delta^{13}\text{C}$ curves fit reasonably well within
424 the global records (Figure 3B, D and F). In the global context, a shift towards more positive values in the $\delta^{13}\text{C}$ at 37 Ma
425 demonstrates a carbon cycle perturbation. The subsequent decrease towards more positive values in the late-Eocene is
426 coeval with the global trend and also coincides with the productivity changes. One possible explanation is that the
427 marine organic carbon burial is increased, preferentially scavenging the light ^{12}C from the carbon pool.

428 This adds evidence to an event of high productivity during the late-Eocene. However, in the Indian Sector and
429 afterwards in the Atlantic Sector of the Southern paleo Ocean, the local $\delta^{13}\text{C}$ does not follow the secular trend. This
430 argues that ocean circulation also changes along with productivity.

431 4.3 Oceanographic Circulation Drivers of the Late Eocene Productivity Change

432 We propose that the main cause for the productivity increase observed in the late Eocene is upwelling of nutrient-rich
433 deep waters. Understanding however the physical oceanographic mechanisms that led to increased upwelling
434 throughout the Southern Ocean requires examining links between the different processes that occurred at that time
435 period. Changes in paleoceanography during the Paleogene were significantly mediated through tectonic re-
436 organisation, such as the Southern Ocean gateways opening (i.e., the Drake Passage and the Tasman Gateway), changes
437 in the Atlantic-Arctic gateway and in the Tethys Seaway.

438 In this context, the Southern Ocean circulation during this time period is still debated due to uncertainties concerning
439 the opening of the gateways that led to the development of the Antarctic Circumpolar Current (ACC). Estimates for the
440 onset of the modern-like ACC have not reached a consensus yet and vary from as early as middle Eocene (ca 41 Ma,



441 Scher & Martin, 2006; ca 35.5 Ma, Stickley et al. 2004) to middle Oligocene (ca 23Ma; Pfuhl and McCave, 2005). This
442 inconsistency suggests that the onset of ACC could have been a gradual or an intermittent change. Further, local proxy
443 records cannot distinguish between regionally developed fronts and true circumpolar, i.e. ACC flow.

444 In addition to $\delta^{18}\text{O}$ and $\delta^{13}\text{C}$, ϵNd has been used to identify circulation changes and water masses exchange through the
445 Eocene (Scher and Martin, 2004, 2008; Scher et al., 2014; Huck et al., 2017; Wright et al., 2018). Nd isotopes are one of
446 the most robust tracers of water mass origin (Frank, 2002). The residence time of Nd in oceans is much shorter (300 -
447 1000 years) than ocean mixing time and is thus distinct at a given location. Further, the isotope composition of the Nd
448 ocean budget is solely determined by terrigenous contribution. The latter is balanced by Nd sinks that remove Nd
449 quantitatively, yet this only influences the net budget and thus the magnitude and/or swiftness of changes to the ϵNd
450 composition. However, mixing of water masses, e.g. through lateral or vertical mixing, can also cause changes as long
451 as they occur more rapidly than the residence times.

452 In the late Eocene, starting at 37 Ma, Scher and Martin (2004) found a dramatic positive shift in $\epsilon\text{-Nd}$ values in the
453 Atlantic sector of the SO that they interpreted as the influx of Pacific deep waters, due to its characteristic of more
454 radiogenic (positive) waters, not previously observed in the Atlantic Ocean. Recently published Nd isotope records from
455 the Kerguelen Plateau (Wright et al., 2018) revealed a long-term negative trend during the late Eocene, which also
456 suggests that the water mass mixing between the Pacific and Atlantic preceded 36 Ma. ϵNd (t) records from the
457 Kerguelen Plateau in fact showed values comparable to modern CDW during the Oligocene, inferring water mass
458 composition similar to the present day. Thus, Nd isotope data support at least partial opening of Drake Passage by the
459 late Eocene (before 36 Ma), consistent with plate tectonic reconstructions (Livermore et al., 2005, 2007). Regardless of
460 the depth, Neodymium isotope evidence for late Eocene opening of the Drake Passage suggests that increased fetch for
461 surface flow and changing deep water composition could have had changes in the surface water conditions in the South
462 Atlantic sector of the late Eocene Southern Ocean.

463 This has been explicitly demonstrated in a recent modelling study conducted by Toumoulin et al. (2020). They
464 demonstrate that the Drake Passage opening, even at shallow depth, notably connects prior regional frontal systems
465 together, thereby allowing the formation of a proto-ACC; and has a strong effect on the Southern Ocean Eocene water
466 mass structure, inducing ocean cooling in most of the Southern Hemisphere. These temperature changes are not linear
467 and differ from one region to another, with DP opening causing changes in the mixed layer depths and provoking
468 different responses in the Atlantic and Indian Sectors of the SO. In the Atlantic and Indian Ocean sectors in particular,
469 very deep seasonal mixing (several hundred meters) over broad areas of the entire region is replaced by more moderate
470 levels of mixing (generally ca 200 m or less), except near the proto-polar front region, where seasonal mixing of 300-
471 400 m still occurs. Vila et al. 2014 have found nannofossil assemblages characteristic of cool sea surface waters in the
472 late-Eocene in Kerguelen Plateau samples Cooler temperatures are coeval with the paleoceanographic re-organization
473 and intensified upwelling that we infer for this time period, while differences in the depth of the mixed layers between
474 ocean basins may explain the different magnitude of export productivity observed in the Atlantic and Indian sectors of
475 the SO.

476 The wind-driven eastward flow and the characteristic fronts of the modern ACC support the upwelling of nutrient-rich
477 water to the surface and consequently high levels of productivity. On the balance of evidence, it seems that the export
478 productivity seen in our data in the late Eocene is likely to have occurred in response to a proto-ACC front's
479 development and its associated upwelling. The inferred onset of a proto-ACC in the late Eocene and our finding of
480 increased upwelling fits the hypothesis that ACC type circulation itself helps drive the AMOC circulation (Toggweiler



481 and Bjornsson, 2000; Katz et al., 2011; Sarkar et al., 2019). A proto-ACC causes SO upwelling, and thus provides
482 support for increasing AMOC-like circulation in the late Eocene as an additional cause of increased upwelling as a
483 causative mechanism of the export productivity event. Temperature asymmetry between Northern and Southern
484 Hemisphere and comparisons between benthic $\delta^{13}\text{C}$ records provide evidence for the strengthening of the AMOC in the
485 late Eocene (Elsworth et al., 2017).

486 **4.4 Eocene-Oligocene Boundary Productivity Changes**

487 The earliest Oligocene, following the EOT, has been suggested as a period of a significant rise in biological productivity
488 in high southern latitudes (Diester-Haass, 1995, 1996; Diester-Haass and Zahn, 1996, 2001). However, in contrast to the
489 late Eocene event, the export productivity changes across the Eocene-Oligocene boundary observed in our study were
490 not always concurrent between the sites investigated (Figure 2). In the Atlantic sites, export productivity increases and
491 decreases several times from the late Eocene to early Oligocene. We thus argue that the fluctuations in export
492 productivity that occurred in the Southern Ocean during this global climatic re-organization are more strongly
493 modulated by local parameters, whereas the late Eocene productivity event is more uniform and reflects the global re-
494 organization of ocean circulation. If the trends observed in export productivity across the EOT were regulated only by
495 global, or at least regional temperature and circulation changes, then we would observe significant changes also in the
496 Indian sector of the Southern Ocean. It seems however that productivity increase was more pronounced in the Atlantic
497 sector of the Southern Ocean.

498 Today, the Southern Ocean (SO) has a frontal system that strongly impacts circulation, primary productivity and the
499 entire climate system (Chapman et al., 2020). The Antarctic Polar Front (APF) is particularly important for controlling
500 nutrient distribution. Latitudinal variations of the APF for example have been shown to alter regional productivity over
501 the glacial cycles (Kim et al., 2014, Thole et al., 2019). The causes of the lack of significant export productivity changes
502 in the Indian sector of the Southern Ocean during the early Oligocene after the Eocene-Oligocene boundary are unclear.
503 The Kerguelen Plateau may not have been located in a position favourable to nutrient-rich upwelling. In addition, the
504 regional frontal migration may have been more intense in the Atlantic sector compared to the Indian sector of the SO.

505 **4.5 A Scenario for Southern Ocean Productivity and Circulation Change in the Late Eocene**

506 The patterns of productivity change seen in our study can be placed in an (admittedly speculative) scenario, which is at
507 least compatible with prior studies and modelling of conditions in the late Eocene austral ocean region and Antarctica.
508 In the earliest interval covered in our study (ca 40-38 Ma) productivity was in most sites fairly low (Figure 5a). At this
509 time there is little evidence for significant influx of Pacific waters into the Atlantic, and the Drake Passage is thus
510 assumed to be effectively closed to ocean circulation.

511 During the 38-36 Ma interval, evidence summarised by Scher et al. (2014) suggests that a significant, if transient,
512 glaciation event occurred on the Antarctic continent - the Priabonian oxygen maximum, or PriOM. If sufficient in
513 magnitude this would have significantly affected circulation throughout the austral ocean region, with strengthened
514 temperature gradients, stronger circumpolar circulation, and increased upwelling (Goldner et al, 2014). This would
515 account both for the substantial increase in productivity, and the broad geographic extent of the increase seen in our data
516 (Figure 5b). The cause of this glaciation event is unknown, but may be related in part to the trend in the late Eocene
517 towards lower atmospheric $p\text{CO}_2$ interacting with orbital fluctuations in polar insolation as explored in model
518 simulations by Van Breedam et al. (2022).



519 With the end of transient glaciation, atmospheric forcing of ocean circulation would have declined, and with it the high
520 levels of productivity seen in our data (Figure 5c). However, by this time (ca 36-34 Ma) the Nd isotope data suggests
521 that a significant influx of Pacific water was reaching the South Atlantic sector of the austral ocean (Scher and Martin,
522 2004), and consequently, the Drake Passage must have been at least partially open. This would have resulted in, if not as
523 strong as during the PriOM, nonetheless stronger circumpolar circulation in a proto-ACC, increased upwelling, and
524 increased nutrient availability from Pacific-sourced deep waters. The locus of high productivity would have become
525 however more centered near the proto-ACC, which at that time, according to the model results of Toumoulin et al.
526 (2020) was located a few degrees north of the current location of the ACC. The high productivity and accumulation of
527 biogenic opal seen at Site 1090, fortuitously located at this time in this region can be thus be explained, as can the lower
528 relative productivity of Site 689, located much further to the south and thus outside the region primarily influenced by
529 the proto-ACC system.

530 Lastly, at the E/O boundary itself (Figure 5d), the well known major shifts in oxygen isotopes signal the formation of a
531 full continental ice-sheet, which would have in turn driven a renewed increase in circumpolar ocean circulation - a full,
532 if early form of the ACC, and dramatically increased levels of productivity, again however primarily near the ACC
533 region.

534 **4.6 Possible Implications to the EOT Global Cooling**

535 Our $p\text{CO}_2$ compilation shows that carbon dioxide levels declined gradually from ca 1200 ppm in the late Eocene to ca
536 750 ppm across the EOT (Figure 4 and Figure S7). There are different processes involved in the oceanic uptake of CO_2 .
537 The solubility pump is a physico-chemical process that promotes gas transfer between atmosphere and sea water in order
538 to achieve chemical equilibrium. This process depends on temperature, in which the solubility increases as temperature
539 decreases. Evidence for cooling of surface waters observed in the Southern Ocean (Liu et al., 2009; Hutchinson et al.,
540 2021) could have favoured the ability to dissolve atmospheric CO_2 , thus being an important contributor to the
541 drawdown of $p\text{CO}_2$ during the late-Eocene.

542 Silicate weathering has been suggested to play an essential role in regulating CO_2 across the EOT (Zachos and Kump,
543 2005). On geologic time scales, chemical silicate weathering is considered to modulate atmospheric CO_2 levels through
544 a negative feedback mechanism (Berner et al., 1983). Weathering of silicate rocks is a source of alkalinity to the oceans
545 and thus a sink for atmospheric CO_2 , thereby influencing global climate. Increasing silicate weathering increases
546 primary productivity through the delivery of nutrients to the ocean. Intensified weathering is supported by Os isotope
547 records, showing an anomaly before the EOT, at ca 35.5Ma (Dalai et al., 2006).

548 The potential effects of enhanced export productivity could have modulated these changes in CO_2 because it removes
549 organic carbon from the surface ocean and transport it into the deep ocean, and thus via sequestration is a mechanism
550 that contributes to the decline of atmospheric carbon dioxide and intensifies the cooling trend. Therefore, enhanced
551 productivity in the late-Eocene and at Eocene-Oligocene transition recorded in our study is a potential candidate that
552 may have provided important positive feedback to the $p\text{CO}_2$ decline.

553 Despite some modelling studies showing that circulation changes were not the main factor in driving the cooling and
554 glaciation on Antarctica (e.g. Huber et al., 2004; Huber and Not 2006; Sijp et al., 2011), sea surface temperature
555 decreased affecting the atmosphere-ocean CO_2 equilibrium. A succession of events may have contributed to the
556 evolution of climate: thermal isolation of Antarctica, glaciers formation, increasing intensity of silicate weathering,
557 together with upwelling of nutrient rich and cold deep waters, leading to higher solubility pump and high biological



558 productivity, then declining $p\text{CO}_2$. Moreover, because the Atlantic Meridional Overturning Circulation (AMOC) affects
559 the distribution of tracers such as temperature, dissolved inorganic carbon (DIC), alkalinity and nutrients (Boot et al.,
560 2021), the strengthening of AMOC could explain the further decrease in atmospheric CO_2 via biological export
561 productivity. Elsworth et al., (2017), for example, suggest that enhanced weathering is driven by intensified AMOC in
562 the latest Eocene due to increasing AMOC causing differential global distribution and increase of surface temperatures
563 and precipitation over land areas. These factors together suggest that E-O changes in AMOC also may play an important
564 role as a driver of CO_2 decline.

565 Taken together, the above processes indicate that a variety of positive feedbacks contributed to Antarctic glaciation from
566 about 37 Ma onwards. Recent evidence suggests that continental-scale Antarctic glaciation initiated in the late Eocene
567 (Scher et al., 2014; Carter et al., 2017). Our results indicate that significant changes in Southern Ocean export
568 productivity preceded the E/O boundary by approximately 3 million years. These trends are likely to be a response to
569 the combination of the intensified processes that had been in place since the late Eocene, and suggest that biological
570 productivity played an important role in the drawdown of $p\text{CO}_2$ levels. The CO_2 fixation by phytoplankton and carbon
571 export to the seafloor increased via biological pump may have contributed to decrease atmospheric CO_2 through a
572 positive feedback and, thus boosting the cooling trend. The establishment of Antarctic glaciation may have been
573 influenced significantly by enhanced productivity. What remains unclear is the biological drivers (plankton) of this
574 productivity change and their role in the long-term evolution of global climate change.

575 **4.7 Limitations and Future Directions**

576 Our study has numerous limitations. Our data on paleoproductivity does not cover the full time interval in all of the sites
577 studied, and our geographic coverage is still incomplete. In particular, we have not examined sections from the Pacific
578 sector, or the influence of the Tasman gateway. Most of our interpretations are based on a single productivity proxy -
579 biogenic Barium. While this proxy is well established and gives coherent results in our study, productivity proxies are
580 known to have complex behaviours, and results using different proxies might be at least somewhat different. Our
581 estimates of how much elevated late Eocene Southern Ocean productivity might have affected global carbon
582 sequestration is only a rough estimate of potential magnitude and much more detailed study of both actual sequestration
583 values in sediment, and the impact on atmospheric $p\text{CO}_2$ are still needed. Our interpretative scenario attributing
584 productivity changes to a combination of Drake Passage opening and continental scale glaciation on Antarctica are
585 purely qualitative and need further study. Despite these limitations, our study sheds new light on the late Eocene
586 oceanic precursors of the Eocene-Oligocene glaciation event - the most dramatic climate change of the Cenozoic.

587 **5 Conclusions**

588 Our bio-Ba data provide important records of the Southern Ocean productivity history across the EOT. These data show
589 that export productivity increased significantly in the late Eocene in the Southern Ocean and was affected by ocean
590 circulation changes. The development of a regionally varying circumpolar polar flow (proto-ACC) and the associated
591 frontal system is likely to have contributed to the enhanced productivity in the Southern Ocean through the
592 intensification of upwelling (H1).

593 Our results show that increasing Southern Ocean productivity in the late Eocene to earliest Oligocene is correlated to
594 global changes in atmospheric $p\text{CO}_2$ and carbon isotope proxies for organic carbon extraction. This finding points
595 toward a potential positive climate system feedback, involving ocean circulation changes, enhanced export productivity



595 and drawdown of atmospheric CO₂. Although studies have the inclination to point to a dominant mechanism (ocean
596 gateway opening vs pCO₂ decline) for causing the initiation of Antarctica glaciation, each mechanism plays a different
597 role and has associated complex feedbacks.. Our study points toward a climate feedback system involving ocean
598 circulation, thermal isolation and biological productivity, where several mechanisms are interconnected and cannot be
599 considered separately. Openings of gateways led to the development of a circumpolar flow, promoting cooling and
600 increased upwelling that contributed to ocean carbon pumps and promotes the decline of atmospheric carbon dioxide.

601 **Data Availability**

602 The supplementary information related to this article is available in the Supplement, the raw data will be available upon
603 publication in an open-access database (PANGAEA: <https://www.pangaea.de>).

604 **Author Contributions**

605 The manuscript was designed and written by GRF in collaboration with DL. DL updated age models. GRF prepared all
606 the samples for geochemical analyses. JS run barium and aluminum analyses. US generated carbon and oxygen stable
607 isotope data. pCO₂ data and neodymium isotopes data were compiled by GRF. Biogenic barium was calculated by GRF.
608 All authors contributed to editing the manuscript.

609 **Competing Interests**

610 The authors declare that they have no conflict of interest.

611 **Acknowledgments**

612 This study was funded by the Federal Ministry of Education and Research (BMBF) under the “Make our Planet Great
613 Again, German Research Initiative”, grant number 57429681, implemented by the German Academic Exchange Service
614 (DAAD).

615 **References**

- 616 Anagnostou, E., John, E. H., Edgar, K. M., Foster, G. L., Ridgwell, A., Inglis, G. N., Pancost, R. D., Lunt, D. J., and
617 Pearson, P. N. Changing atmospheric CO₂ concentration was the primary driver of early Cenozoic climate: *Nature*, v.
618 533, pp. 380-384. <https://doi.org/10.1038/nature17423>, 2016.
- 619 Anagnostou, E., John, E. H., Babila, T.L., Sexton, P. F., Ridgwell, A., Lunt, D.J., Pearson, P.N., Chalk, T.B., Pancost,
620 R.D. and Foster, G.L. Proxy evidence for state-dependence of climate sensitivity in the Eocene greenhouse. *Nature*
621 *Communications*, 11, 4436 (2020). <https://doi.org/10.1038/s41467-020-17887-x>, 2020.
- 622 Anderson, L.D. & Delaney, M.L. Middle Eocene to early Oligocene paleoceanography from Agulhas Ridge, Southern
623 Ocean (Ocean Drilling Program Leg 177, Site 1090). *Paleoceanography and Paleoclimatology*, 20, 1.
624 <https://doi.org/10.1029/2004PA001043>, 2005.
- 625 Anderson, J.B., Warny, S., R.A. Askin, J.S. Wellner, S.M. Bohaty, A.E. Kirshner, D.N. Livsey, A.R. Simms, T.R. Smith,
626 W. Ehrmann, L.A. Lawver, D. Barbeau, S.W. Wise, D.K. Kulhanek, F.M. Weaver, W. Majewski. Progressive Cenozoic
627 cooling and the demise of Antarctica's last refugium *PNAS*, 108, pp. 11356-11360, 2011.
- 628 Arrhenius, S. On the influence of carbonic acid in the air upon the temperature of the ground. *Philosophical Magazine*
629 *and Journal of Science*, 5, v.41, 237-276, 1986.
- 630 Aubry, M.P. Late Paleogene Calcareous nannoplankton evolution: a tale of climatic deterioration In: Prothero, D.R.,
631 Berggren, W.A. (Eds.), *Eocene/Oligocene Climatic and Biotic Evolution*, Princeton University Press, Princeton, NJ,
632 pp.272-309, 1992.



- 633 Baldauf, J. G., & Barron, J. A. 29. Diatom Biostratigraphy: Kerguelen Plateau and Prydz Bay regions of the Southern
634 Ocean. In: Barron, J., Larsen, B. et al. (1991) Proceedings of the Ocean Drilling Program, Scientific Results, v 119,
635 1991
- 636 Barker, P.E., Kennett, J.P., et al. Proc. ODP, Init. Repts., 113: College Station, TX (Ocean Drilling Program).
637 doi:10.2973/odp.proc.ir.113.1988.
- 638 Barker, P.F. Scotia Sea regional tectonic evolution: implications for mantle flow and palaeocirculation. *Earth-Science*
639 *Reviews*, 55, 1-39 [https://doi.org/10.1016/S0012-8252\(01\)00055-1](https://doi.org/10.1016/S0012-8252(01)00055-1), 2001
- 640 Barron, J., Larsen, B., et al. Proc. ODP, Init. Repts., 119: College Station, TX (Ocean Drilling Program).
641 doi:10.2973/odp.proc.ir.119.1989.
- 642 Beerling, D., Royer, D. Convergent Cenozoic CO₂ history. *Nature Geoscience*, 4, 418–420
643 <https://doi.org/10.1038/ngeo1186>, 2011.
- 644 Berggren, W.A., Kent, D.V., Swisher, C.C., III, and Aubry, M.P. A revised Cenozoic geochronology and
645 chronostratigraphy, in Berggren, W.A., et al., eds., *Geochronology, time scales and global stratigraphic correlation:*
646 *Framework for an historical geology: SEPM (Society for Sedimentary Geology) Special Publication 54*, p. 129–212,
647 1995.
- 648 Berner, R. A., Lasaga, A. C. & Garrels, R. M. The carbonate-silicate geochemical cycle and its effect on atmospheric
649 carbon dioxide over the past 100 million years. *Am. J. Sci.* 283, 641–683, 1983.
- 650 Billups, K., Channell, J.E.T. and Zachos, J. Late Oligocene to early Miocene geo- chronology and paleoceanography
651 from the subantarctic South Atlantic, *Paleoceanography*, 17(1), 1004. doi:10.1029/2000PA000568, 2002.
- 652 Bijl, P.K., Houben, A. J. P., Schouten, S., Bohaty, S. M., Sluijs, A., Reichert, G.-J., Sinninghe Damste, J.S., and
653 Brinkhuis, H. Transient Middle Eocene atmospheric CO₂ and temperature variations, *Science*, 330, 819-821, 2010.
- 654 Bohaty, S. M. and Zachos, J. C. Significant Southern Ocean warming event in the late middle Eocene, *Geology*, 31,
655 1017–1020, <https://doi.org/10.1130/G19800.1>, 2003.
- 656 Bohaty, S. M., Zachos, J.C., and Delaney, M.L. Foraminiferal Mg/Ca evidence for Southern Ocean cooling across the
657 Eocene-Oligocene transition, *Earth Planet. Sci. Lett.*, 317–318, 251–261, 2012.
- 658 Boot, D., Von Der Heydt, A.S., and Dijkstra, H.A. Effect of the Atlantic Meridional Overturning Circulation on
659 Atmospheric pCO₂ variations. *Earth System Dynamics*, <https://doi.org/10.5194/esd-13-1041-2022>, 2022
- 660 Carter, L., McCave, I.N., Williams, M.J.M. Chapter 4 Circulation and Water Masses of the Southern Ocean: A Review,
661 *Developments in Earth and Environmental Sciences*, Elsevier, v. 8, 85-114, [https://doi.org/10.1016/S1571-](https://doi.org/10.1016/S1571-9197(08)00004-9)
662 [9197\(08\)00004-9](https://doi.org/10.1016/S1571-9197(08)00004-9), 2008.
- 663 Carter, A., Riley, T.R., Hillenbrand, C.D., Rittner, M. Widespread Antarctic glaciation during the Late Eocene, *Earth*
664 *and Planetary Science Letters*, 458, 49-57, <https://doi.org/10.1016/j.epsl.2016.10.045>, 2017.
- 665 Channell, J. E. T., Galeotti, S., Martin, E.E., Billups, K., Scher, H.D., and Stoner, J.S. Eocene to Miocene
666 magnetostratigraphy, biostratigraphy and chemostratigraphy at ODP Site 1090 (sub-Antarctic South Atlantic), *Geol.*
667 *Soc. Am. Bull.*, 115, 607–623, 2003.
- 668 Chapman, C.C., Lea, M.A., Meyer, A. Defining Southern Ocean fronts and their influence on biological and physical
669 processes in a changing climate. *Nature Climate Change*, 10, 209–219, <https://doi.org/10.1038/s41558-020-0705-4>,
670 2020.
- 671 Clark, W. C. (ed.). *Carbon Dioxide Review: 1982*, p. 468, Oxford University Press, New York, 1982.
- 672 Cooke, P.J., Nelson, C.S., Crundwell, M.P., Spiegler, D. Bolboforma as monitors of Cenozoic palaeoceanographic
673 changes in the Southern Ocean, *Palaeogeography, Palaeoclimatology, Palaeoecology*, Volume 188, Issues 1–2, 73-100,
674 [https://doi.org/10.1016/S0031-0182\(02\)00531-X](https://doi.org/10.1016/S0031-0182(02)00531-X), 2002.
- 675 Coxall, H.K., Wilson, P.A., Pälike, H., Lear, C.H., Backman, J. Rapid stepwise onset of Antarctic glaciation and deeper
676 calcite compensation in the Pacific Ocean. *Nature* 433, 53–57. <https://doi.org/10.1038/nature03135>, 2005.
- 677 Coxall, H., Pearson, P.N. The Eocene-Oligocene transition, In: Williams, M., Haywood, A.M., Gregory, F.J., Schmidt,
678 D.N. (Eds.), *Deep-Time Perspectives on Climate Change: Marrying the Signal from Computer Models and Biological*
679 *Proxies*. pp. 351–387, 2007.
- 680 Coxall, H. K., & Wilson, P. A. Early Oligocene glaciation and productivity in the eastern equatorial Pacific: Insights
681 into global carbon cycling, *Paleoceanography*, 26, PA2221, <https://doi.org/10.1029/2010PA002021>, 2011.
- 682 Coxall, H.K., Huck, C.E., Huber, M. Export of nutrient rich Northern Component Water preceded early Oligocene
683 Antarctic glaciation. *Nature Geoscience* 11, 190–196, 2018.
- 684 Cramer, B. S., J. R. Toggweiler, J. D. Wright, M. E. Katz, and K. G. Miller. Ocean overturning since the Late
685 Cretaceous: Inferences from a new benthic foraminiferal isotope compilation, *Paleoceanography*, 24, PA4216,
686 doi:10.1029/2008PA001683, 2009.
- 687 Dalai, T.K. et al. The Late Eocene 187Os/188Os excursion: Chemostratigraphy, cosmic dust flux and the Early
688 Oligocene glaciation. *Earth and Planetary Science Letters*, 241(3-4), 477-492,
689 <https://doi.org/10.1016/j.epsl.2005.11.035>, 2006.
- 690 De Baar, H., de Jong, J., Bakker, D. et al. Importance of iron for plankton blooms and carbon dioxide drawdown in the
691 Southern Ocean. *Nature* 373, 412–415 <https://doi.org/10.1038/373412a0>, 1995.



- 692 DeConto, R. & Pollard, D. Rapid Cenozoic glaciation of Antarctica induced by declining atmospheric CO₂. *Nature* 421,
693 245–249. <https://doi.org/10.1038/nature01290>, 2003.
- 694 DeConto RM, Pollard D, Wilson PA, Palike H, Lear CH, Pagani M. Thresholds for Cenozoic bipolar glaciation.
695 [doi:10.1038/nature07337](https://doi.org/10.1038/nature07337), 2008.
- 696 Diekmann, B., Kuhn, G., Gersonde, R., Mackensen, A. Middle Eocene to early Miocene environmental changes in the
697 sub-Antarctic Southern Ocean: evidence from biogenic and terrigenous depositional patterns at ODP Site 1090, *Global*
698 *and Planetary Change*, Volume 40, Issues 3–4, Pages 295–313, <https://doi.org/10.1016/j.gloplacha.2003.09.001>, 2004.
- 699 Diester-Haass, L. Late Eocene-Oligocene sedimentation in the Antarctic Ocean, Atlantic Sector (Maud Rise, ODP leg
700 113, Site 689), Development of surface and bottom water circulation, in *The Antarctic Paleoenvironment: A Perspective*
701 *on Global Change, Part 1, Antarct. Res. Ser.*, vol. 56, edited by J. P. Kennett, and D. A. Warnke, pp. 185– 202, AGU,
702 Washington, D. C, 1992.
- 703 Diester-Haass, L. Middle Eocene to early Oligocene Paleoceanography of the Antarctic Ocean (Maud Rise, ODP Leg
704 113, Site 689): change from a low to a high productivity ocean. *Paleogeography, Paleoclimatology, Paleoecology*, 113,
705 311–334. [https://doi.org/10.1016/0031-0182\(95\)00067-V](https://doi.org/10.1016/0031-0182(95)00067-V), 1995.
- 706 Diester-Haass, L. Late Eocene-Oligocene paleoceanography in the southern Indian Ocean (ODP Site 744). *Marine*
707 *Geology* 130, 99–119, 1996.
- 708 Diester-Haass, L & Zahn, R. Eocene-Oligocene transition in the Southern Ocean: History of water mass circulation and
709 biological productivity, *Geology*, 24, 163–166. 1996.
- 710 Diester-Haass, L & Zahn, R. Paleoproductivity increase at the Eocene-Oligocene climatic transition: ODP/DSDP Sites
711 763 and 592. *Paleoceanography, Paleoclimatology, Paleoecology*, 172, 153–170. [https://doi.org/10.1016/S0031-](https://doi.org/10.1016/S0031-0182(01)00280-2)
712 [0182\(01\)00280-2](https://doi.org/10.1016/S0031-0182(01)00280-2), 2001.
- 713 Diester-Haass, L. & Zachos, J. The Eocene-Oligocene transition in the Equatorial Atlantic (ODP Site 925);
714 paleoproductivity increase and positive $\delta^{13}C$ excursion. In Prothero, D.R.; Ivany, L. C.; Nesbitt, E. A. (eds) *From*
715 *greenhouse to icehouse; the marine Eocene-Oligocene transition*, Columbia University Press, New York, NY, United
716 States (USA), 2003.
- 717 Diester-Haass, L., & Faul, K. Paleoproductivity reconstructions for the Paleogene Southern Ocean: A direct comparison
718 of geochemical and micropaleontological proxies. *Paleoceanography and Paleoclimatology*, 34(1), 79– 97.
719 <https://doi.org/10.1029/2018PA003384>, 2019.
- 720 Douglas, P.M.J., Affek, H.P., Ivany, L.C., Houben, A.J.P., Sijp, W.P., Sluijs, A., Schouten, S., Pagani, M. Pronounced
721 zonal heterogeneity in Eocene southern high-latitude sea surface temperatures. *PNAS*, 111 (18) 6582–6587
722 <https://doi.org/10.1073/pnas.1321441111>, 2014.
- 723 Dutkiewicz, A., Müller, R.D. The carbonate compensation depth in the South Atlantic Ocean since the Late Cretaceous.
724 *Geology*, 49 (7): 873–878. <https://doi.org/10.1130/G48404.1>, 2021.
- 725 Dymond, J., Suess, E. and Lyle, M. Barium in Deep-Sea Sediment: A Geochemical Proxy for Paleoproductivity.
726 *Paleoceanography and Paleoclimatology*, 7(2), 163–181. <https://doi.org/10.1029/92PA00181>, 1992.
- 727 Elsworth, G., Galbraith, E., Halverson, G. et al. Enhanced weathering and CO₂ drawdown caused by latest Eocene
728 strengthening of the Atlantic meridional overturning circulation. *Nature Geoscience* 10, 213–216).
729 <https://doi.org/10.1038/ngeo2888>, 2017.
- 730 Faul K. L., Delaney, M. L. A comparison of early Paleogene export productivity and organic carbon burial flux for
731 Maud Rise, Weddell Sea, and Kerguelen Plateau, south Indian Ocean. *Paleoceanography*, v.25, 3214, 2010.
- 732 Falkowski P., Scholes R.J., Boyle E., Canadell J., Canfield D., Elser J., Gruber N., Hibbard K., Högberg P., Linder S.,
733 Mackenzie F.T., Moore III B., Pedersen T., Rosenthal Y., Seitzinger S., Smetacek V., Steffen W. The global carbon
734 cycle: a test of our knowledge of earth as a system. *Science*, 290, 291–296. [doi: 10.1126/science.290.5490.291](https://doi.org/10.1126/science.290.5490.291). PMID:
735 11030643, 2000.
- 736 Florindo, F. and Roberts, A. P. Eocene-Oligocene magnetobiochronology of ODP Sites 689 and 690, Maud Rise,
737 Weddell Sea, Antarctica. *Geological Society of America Bulletin*, 117(1), 46–. [doi:10.1130/b25541.1](https://doi.org/10.1130/b25541.1), 2005
- 738 Foster, G.; Royer, D. and Lunt, D. Future climate forcing potentially without precedent in the last 420 million years.
739 *Nature Communications*, 8, 14845. <https://doi.org/10.1038/ncomms14845>, 2017.
- 740 Frank, M. Radiogenic isotopes: tracers of past ocean circulation and erosional input. *Rev. Geophys.* 40, 1001.
741 [doi:10.1029/2000RG000094](https://doi.org/10.1029/2000RG000094), 2002.
- 742 Galeotti, S., Coccioni, R., Gersonde, R. Middle Eocene–Early Pliocene Subantarctic planktic foraminiferal
743 biostratigraphy of Site 1090, Agulhas Ridge, *Marine Micropaleontology*, 45, 3–4, 357–381,
744 [https://doi.org/10.1016/S0377-8398\(02\)00035-X](https://doi.org/10.1016/S0377-8398(02)00035-X), 2002.
- 745 Gersonde, R., Hodell, B.A., Blum, P., and Shipboard Scientific Party. Leg 177 summary, *Proc. Ocean Drill. Program*,
746 *Initial Rep.*, 177, 1–67, 1999.
- 747 Glass, B.P., Hall, C.M., and York, D. ⁴⁰Ar/³⁹Ar laser probe dating of North American tektite fragments from Barbados
748 and the age of the Eocene-Oligocene boundary: *Chemical Geology*, v. 59, p. 181–186., 1996.
- 749 Goldner, A., Herold, N. and Huber, M. Antarctic glaciation caused ocean circulation changes at the Eocene-Oligocene
750 transition, *Nature*, 511(7511), 574–577, [doi:10.1038/nature13597](https://doi.org/10.1038/nature13597), 2014.



- 751 Gradstein, F. M., Ogg, J. G., Schmitz, M., & Ogg, G. The Geological Time Scale 2012 (pp. 1176). Oxford, UK:
752 Elsevier, 2012.
- 753 Gruber, N., Landschützer, P., Lovenduski, N.S. The Variable Southern Ocean Carbon Sink. *Annual Review of Marine*
754 *Science*, 11, 159-186. <https://doi.org/10.1146/annurev-marine-121916-063407>, 2019.
- 755 Hayes, C.T.; Costa, K.M.; Anderson, R.F.; Calvo, E.; Chase, Z.; Demina, L.L.; Dutay, J.; German, C.R.; Heimbürger-
756 Boavida, L.; Jaccard, S.L.; et al. Global Ocean Sediment Composition and Burial Flux in the Deep Sea. *Global*
757 *Biogeochem. Cycles* 35, 2021.
- 758 Henehan, M.; Edgar, K.M.; Foster, G.L., Penman, D.E.; Hull, P.M.; Greenop, R.; Anagnostou, E.; Pearson, P.N.
759 Revisiting the Middle Eocene Climatic Optimum “Carbon Cycle Conundrum” with New Estimates of Atmospheric
760 pCO₂ from Boron Isotopes. *Paleoceanography and Paleoclimatology*. 35(6). <https://doi.org/10.1029/2019PA003713>,
761 2020.
- 762 Houben, A.J.P., van Mourik, C.A., Montanari, A., Coccioni, R., Brinkhuis, H. The Eocene–Oligocene transition:
763 Changes in sea level, temperature or both? *Palaeogeography, Palaeoclimatology, Palaeoecology*. 335–336,p 75-83
764 <https://doi.org/10.1016/j.palaeo.2011.04.008>, 2012.
- 765 Huber, B.T. and Quillevere, F. Revised Paleogene Planktonic Foraminiferal biozonation for the Austral realm. *Journal*
766 *of Foraminiferal Research*, 35(4), 299-314., 2005.
- 767 Huber, M., Brinkhuis, H., Stickley, C.E., Döös, K., Sluijs, A., Warner, J., Schellenberg, S.A. and Williams, G.L. Eocene
768 circulation of the Southern Ocean: Was Antarctica kept warm by subtropical waters? *Paleoceanography* 19,
769 doi:10.1029/2004PA001014, 2004.
- 770 Huber, M. and Nof, D. The ocean circulation in the southern hemisphere and its climatic impacts in the Eocene.
771 *Palaeogeography, Palaeoclimatology, Palaeoecology* 231, 9-28, 2006.
- 772 Huck, C. E., van de Flierdt, T., Bohaty, S. M. and Hammond, S. J. Antarctic climate, Southern Ocean circulation
773 patterns, and deep-water formation during the Eocene. *Paleoceanography*, 32, 674– 691.
774 <https://doi.org/10.1002/2017PA003135>, 2017.
- 775 Hutchinson, D.K., Coxall, H.K., Lunt, D.J., Steinthorsdottir, M., de Boer, A.M. et al. The Eocene-Oligocene transition:
776 A review of marine and terrestrial proxy data, models and model-data comparisons. *Climate of the Past* 17(1), 269-315,
777 2021.
- 778 Inglis, G. N., Farnsworth, A., Lunt, D., Foster, G. L., Hollis, C. J., Pagani, M., Jardine, P. E., Pearson, P. N., Markwick,
779 P., Galsworthy, A. M. J., Raynham, L., Taylor, K. W. R. and Pancost, R. D. Descent toward the Icehouse: Eocene sea
780 surface cooling inferred from GDGT distributions, *Paleoceanography*, 30(7), 1000–1020, doi:10.1002/2014PA002723,
781 2015.
- 782 Inokuchi, H; Heider, F. Paleolatitude of the southern Kerguelen Plateau inferred from the paleomagnetic study of late
783 Cretaceous basalts. In: Wise, SW; Schlich, R; et al. (eds.), *Proceedings of the Ocean Drilling Program, Scientific*
784 *Results, College Station, TX (Ocean Drilling Program)*, 120, 89-96, <https://doi.org/10.2973/odp.proc.sr.120.129.1992>
- 785 IPCC. *Climate Change 2021: The Physical Science Basis. Working Group I Contribution to the Sixth Assessment*
786 *Report of the Intergovernmental Panel on Climate Change. Cambridge University Press, Cambridge, United Kingdom*
787 *and New York, NY, USA, 2391pp, 2021.*
- 788 Katz, M.E., Cramer, B.S., Toggweiler, J.R., Esmay, G., Liu, C., Miller, K.G., Rosenthal, Y., Wade, B.S., Wright J.D.
789 Impact of Antarctic Circumpolar Current Development on Late Paleogene Ocean Structure. *Science*, 332, 1076-1079,
790 2011.
- 791 Kennet, J.P. Cenozoic evolution of Antarctic glaciation, the circum-Antarctic Ocean, and their impact on global
792 paleoceanography. *J. Geophys. Res.*, 82, 3843-3860, 1977.
- 793 Kennett, J.P. and Stott, L.D. Proteus and Proto- Oceanus: ancestral Paleogene oceans as revealed from antarctic stable
794 isotopic results: ODP Leg 113. In: Leg 113. ODP Sci. Res., pp. 865-880, 1990.
- 795 Kim J.H., Crosta, X., Michel, E., Schouten, S., Duprat, J., Damsté, J.S.S. Impact of lateral transport on organic proxies
796 in the Southern Ocean, *Quaternary Research*, 71(2), 246-250. <https://doi.org/10.1016/j.yqres.2008.10.005>, 2009.
- 797 Kim, Yong Sun, Orsi, Alejandro H. On the Variability of Antarctic Circumpolar Current Fronts Inferred from 1992–
798 2011 Altimetry. *Journal of Physical Oceanography* 3054–3071. <https://doi.org/10.1175/JPO-D-13-0217.1>, 2014.
- 799 Kuhlbrodt, T., Griesel, A., Montoya, M., Levermann, A., Hofmann, M., Rahmstorf, S. On the driving processes of the
800 Atlantic meridional overturning circulation. *Rev. Geophys.*, 45, RG2001, doi:10.1029/2004RG000166, 2007.
- 801 Ladant, J.-B., Donnadieu, Y. and Dumas, C. Links between CO₂, glaciation and water flow: reconciling the Cenozoic
802 history 1680 of the Antarctic Circumpolar Current, *Clim. Past*, 10(6), 1957–1966, doi:10.5194/cp-10-1957-2014, 2014.
- 803 Lauretano, V., Kennedy-Asser, A.T., Korasidis, V.A., Wallace, M.W., Valdes, P.J., Lunt, D.J., Pancost, R.D. and naafs,
804 B.D.A. Eocene to Oligocene terrestrial Southern Hemisphere cooling caused by declining pCO₂. *Nature Geoscience* 14,
805 659–664. <https://doi.org/10.1038/s41561-021-00788-z>, 2021.
- 806 Lazarus, D. and Caulet J.P. Cenozoic Southern Ocean reconstructions from sedimentologic, radiolarian, and other
807 microfossil data. In: J.P. Kennett and D.A. Warnke, Eds., *The Antarctic Paleoenvironment: A perspective on global*
808 *change. Pt. 2. Antarctic Research Series*, 60: 145-174, 1994.
- 809 Li, Z., Lozier, M.S., Cassar, N. Linking Southern Ocean Mixed Layer Dynamics to Net Community Production on
810 Various Timescales. *JGR Oceans* 126. <https://doi.org/10.1029/2021JC017537>, 2021.



- 811 Liu, Z., M., Pagani, D., Zinniker, R., DeConto, M., Huber, H., Brinkhuis, S. R., Shah, R. M. Leckie, and Pearson, A.
812 Global cooling during the Eocene – Oligocene climate transition, *Science*, 323, 1187–1190, 2009.
- 813 Livermore, R., Nankivell, Eagles, G. and Morris, P. Paleogene opening of Drake Passage, *Earth Planet. Sci. Lett.*, 236,
814 459–470, 2005.
- 815 Livermore, R., Hillenbrand, C., Meredith, M., and Eagles, G. Drake Passage and Cenozoic climate: an open and shut
816 case?, *Geochem. Geophys. Geosy.*, 8, Q01005, <https://doi.org/10.1029/2005GC001224>, 2007.
- 817 Mackensen, A., and Ehrmann, W.U. Middle Eocene through Early Oligocene climate history and paleoceanography in
818 the Southern Ocean: Stable oxygen and carbon isotopes from ODP Sites on Maud Rise and Kerguelen Plateau, *Mar.*
819 *Geol.*, 108, 1–27, 1992.
- 820 Marino, M. and Flores, J.A. Middle Eocene to early Oligocene calcareous nannofossil stratigraphy at Leg 177 Site
821 1090, *Mar. Micropaleontol.*, 45, 383–398, 2002.
- 822 Martin, E.E. and Haley, B.A. Fossil fish teeth as proxies for seawater Sr and Nd isotopes. *Geochimica et Cosmochimica*
823 *Acta*, 64 (5), 835–847, doi:10.1016/S0016-7037(99)00376-2, 2000.
- 824 Martin, E.E. and Scher, H.D. Preservation of seawater Sr and Nd isotopes in fossil fish teeth: bad news and good news.
825 *Earth and Planetary Science Letters*, 220(1-2), 25–39, [https://doi.org/10.1016/S0012-821X\(04\)00030-5](https://doi.org/10.1016/S0012-821X(04)00030-5), 2004.
- 826 Mazloff, M.R., Heimbach, P., Wunsch, C. An eddy-permitting Southern Ocean state estimate. *J. Phys. Oceanogr.* 40,
827 880–899, 2010.
- 828 Mikolajewicz, U., Maier-Reimer, E., Crowley, T. J. and Kim, K.-Y. Effect of Drake and Panamanian Gateways on the
829 circulation of an ocean model, *Paleoceanography*, 8(4), 409–426, doi:10.1029/93PA00893, 1993.
- 830 Miller, K.G. Janecek, T.R., Katz, M.E., Keil, D.J. Abyssal circulation and benthic foraminiferal changes near the
831 Paleocene/Eocene boundary. *Paleoceanography*, 2(6), 741–761, <https://doi.org/10.1029/PA002i006p00741>, 1987.
- 832 Miller, K.G., Wright, J.D., Katz, M.E., Wade, B., Browning, J.V., Cramer, B.S., and Rosenthal, Y. Climate threshold at
833 the Eocene-Oligocene transition: Antarctic ice sheet influence on ocean circulation, in Koeberl, C., and Montanari, A.,
834 ed., *The Late Eocene Earth Hot house, Icehouse, and Impacts: Geological Society of America Special Paper 452*, p.
835 169–178, doi:10.1130/2009.2452 (11), 2009.
- 836 Moore, J. K., M. R. Abbott, J. G. Richman, W. O. Smith, T. J. Cowles, K. H. Coale, W. D. Gardner, and R. T. Barber.
837 SeaWiFS satellite ocean color data from the Southern Ocean, *Geophys. Res. Lett.*, 26, 1465–1468, 1999.
- 838 Muza, J.P., Williams, D.F., Wise, S.W. Paleogene oxygen record for Deep Sea Drilling Project Sites 511 and 512,
839 subantarctic South Atlantic Ocean: Paleotemperatures, paleoceanographic changes, and the Eocene/Oligocene boundary
840 event. In: Ludwig, WJ; Krashennikov, VA; et al. (Eds.), *Initial Reports of the Deep-Sea Drilling Project (U.S. Govt.*
841 *Printing Office)*, 71, 409–422, <https://doi.org/10.2973/dsdp.proc.71.117.1983>, 1983.
- 842 Najjar, R.G., Nong, G.T., Seidov, D., Peterson, W.H. Modeling geographic impacts on early Eocene ocean temperature,
843 *Geophys. Res. Lett.*, 29 (15), 401–404. <https://doi.org/10.1029/2001GL014438>, 2002.
- 844 Nelson, D.M. & Smith, W. Sverdrup revisited: Critical depths, maximum chlorophyll levels, and the control of Southern
845 Ocean productivity by the irradiance-mixing regime. *Limnol. Oceanogr.* 36, 1650–1661.
846 <https://doi.org/10.4319/lo.1991.36.8.1650>, 1991.
- 847 Nielsen, E.B., Anderson, L.D., Delaney, M.L. Paleoproductivity, nutrient burial, climate change and the carbon cycle in
848 the western equatorial Atlantic across the Eocene/Oligocene boundary. *Paleoceanography*, v 18, n. 3, 1057,
849 doi:10.1029/2002PA000804, 2003.
- 850 O'Brien, C. L., Huber, M., Thomas, E., Pagani, M., Super, J. R., Elder, L. E., Hull, P. M. The enigma of Oligocene
851 climate and global surface temperature evolution. *Proceedings of the National Academy of Sciences Oct 2020*, 117 (41)
852 25302–25309; DOI:10.1073/pnas.2003914117, 2020.
- 853 Orsi, A.H., Whitworth, T., Nowlin, W.D. On the meridional extent and fronts of the Antarctic Circumpolar Current,
854 *Deep Sea Research Part I: Oceanographic Research Papers*, v 42, 5, 641–673, [https://doi.org/10.1016/0967-
855 *0637\(95\)00021-W*, 1995.](https://doi.org/10.1016/0967-0637(95)00021-W)
- 856 Pagani, M., Zachos, J. C., Freeman, K. H., Tipple, B., and Bohaty, S. Marked decline in atmospheric carbon dioxide
857 concentrations during the Paleogene. *Science*, 309 600–603. DOI: 10.1126/science.111006, 2005
- 858 Pagani, M., Huber, M., Liu, Z., Bohaty, S.M., Henderiks, J., Sijp, W., Krishnan, S. & DeConto, R.M. The role of carbon
859 dioxide during the onset of Antarctic glaciation. *Science*, 334, 1261–1264. DOI: 10.1126/science.1203909, 2011.
- 860 Pälike, H., Lyle, M.W., Nishi, H., Raffi, I., Ridgwell, A., Gamage, K., Klaus, A., Acton, G., Anderson, L., Backman, J.,
861 Baldauf, J., Beltran, C., Bohaty, S.M., Bown, P., Busch, W., Channell, J.E.T., Chun, C.O.J., Delaney, M., Dewangan, P.,
862 Dunkley Jones, T., Edgar, K.M., Evans, H., Fitch, P., Foster, G.L., Gussone, N., Hasegawa, H., Hathorne, E.C., Hayashi,
863 H., Herrle, J.O., Holbourn, A., Hovan, S., Hyeong, K., Iijima, K., Ito, T., Kamikuri, S., Kimoto, K., Kuroda, J., Leon-
864 Rodriguez, L., Malinverno, A., Moore, T.C., Murphy, B.H., Murphy, D.P., Nakamura, H., Ogane, K., Ohneiser, C.,
865 Richter, C., Robinson, R., Rohling, E.J., Romero, O., Sawada, K., Scher, H., Schneider, L., Sluijs, A., Takata, H., Tian,
866 J., Tsujimoto, A., Wade, B.S., Westerhold, T., Wilkens, R., Williams, T., Wilson, P.A., Yamamoto, Y., Yamamoto, S.,
867 Yamazaki, T., Zeebe, R.E. A Cenozoic record of the equatorial Pacific carbonate compensation depth, *Nature* 488
868 (7413), 609–615, doi:10.1038/nature11360, 2012.
- 869 Palter, J. B., Sarmiento, J. L., Marinov, I. & Gruber, N. In *Chemical Oceanography of Frontal Zones* (ed. Belkin, I. M.)
870 <https://doi.org/10.1007/978-2013-241> (Springer), 2013.



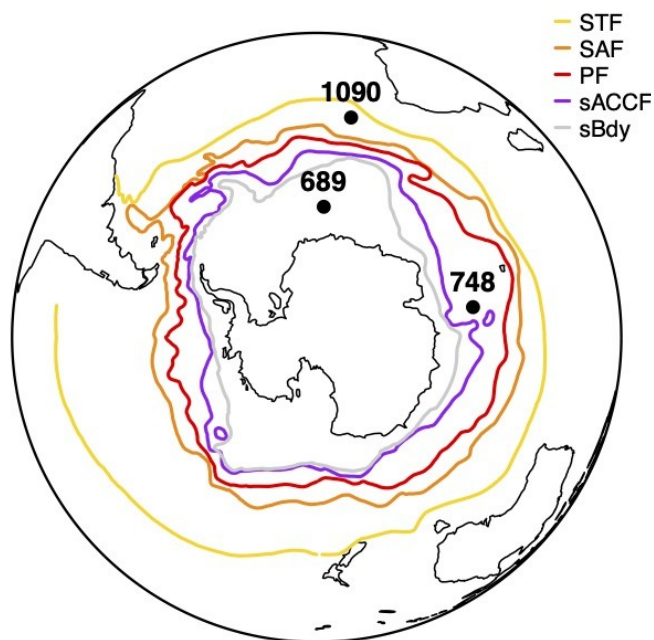
- 871 Park Y. H., Park T., Kim T.W., Lee S.H., Hong C.S., Lee J.H., Rio M.H., Pujol M.I., Ballarotta M., Durand I., Provost
872 C. Observations of the Antarctic Circumpolar Current over the Udintsev Fracture Zone, the narrowest choke point in the
873 Southern Ocean. *Journal of Geophysical Research: Oceans*, -. <https://doi.org/10.1029/2019JC015024>, 2019.
- 874 Pearson, P. & Palmer, M.R. Atmospheric carbon dioxide concentrations over the past 60 million years. *Nature*, 206,
875 695-699, 2000.
- 876 Pearson, P., Foster, G. and Wade, B. Atmospheric carbon dioxide through the Eocene–Oligocene climate transition.
877 *Nature*, 461, 1110–1113. <https://doi.org/10.1038/nature08447>, 2009.
- 878 Persico, D., and Villa, G. High-resolution calcareous nannofossil biostratigraphy and palaeoecology from Eocene-
879 Oligocene sediments, Maud Rise, Weddell Sea, and Kerguelen Plateau, Antarctica: University of Parma, Italy, Abstract
880 9th International Nannoplankton Association Conference, 8th–14th September 2002.
- 881 Persico, D., and Villa, G. Eocene-Oligocene calcareous nannofossils from Maud Rise and Kerguelen Plateau
882 (Antarctica): Palaeoecological and palaeoceanographic implications: *Marine Micropaleontology*, v. 52, p. 153–179, doi:
883 10.1016/j.marmicro.2004.05.002, 2004.
- 884 Piepgras D.J., Wasserburg G.J. Isotopic composition of neodymium in waters from the drake passage. *Science* Jul
885 16;217(4556):207-14. doi:10.1126/science.217.4556.207, 1992.
- 886 Pfuhl, H. A. & McCave, I. N. Evidence for late Oligocene establishment of the Antarctic Circumpolar Current. *Earth
887 and Planetary Science Letters*, 235, 715–728, 2005.
- 888 Prothero, D.R. & Berggren, W.A. *Eocene-Oligocene Climatic and Biotic Evolution*. Princeton Univ. Press, Princeton,
889 NJ, 1992.
- 890 Pusz, A. E., Thunell, R.C. and Miller, K.G. Deep water temperature, carbonate ion, and ice volume changes across the
891 Eocene-Oligocene climate transition, *Paleoceanography*, 26, PA2205, doi:10.1029/2010PA001950, 2011.
- 892 Renaudie, J., Lazarus, D. and Diver, P. NSB (Neptune Sandbox Berlin): An expanded and improved database of marine
893 planktonic microfossil data and deep-sea stratigraphy. *Palaeontologia Electronica*,23(1):a11
894 <https://doi.org/10.26879/1032>, 2020.
- 895 Rintoul, S.R., Hughes, C.W., Olbers, D. Chapter 4.6 The antarctic circumpolar current system, Editor(s): Gerold Siedler,
896 John Church, John Gould, International Geophysics, Academic Press, v.77, 271-XXXVI, 2001.
- 897 Robert, C., Diester Haass, L. and Chamley, H. (2002). Late Eocene Oligocene oceanographic development at southern
898 high latitudes, from terrigenous and biogenic particles: A comparison of Kerguelen Plateau and Maud Rise, ODP Sites
899 744 and 689, *Mar. Geol.*, 191, 37–54, doi:10.1016/S0025-3227(02)00508-X, 2002.
- 900 Roberts, A.P., Bicknell, S.J., Byatt, J., Bohaty, S.M., Florindo, F., and Harwood, D.M. Magnetostratigraphic calibration
901 of Southern Ocean diatom datums from the Eocene-Oligocene of Kerguelen Plateau (Ocean Drilling Program Sites 744
902 and 748): *Palaeogeography, Palaeoclimatology, Palaeoecology*, v. 198, p. 145–168, doi: 10.1016/S0031-0182(03)00397-
903 3, 2003.
- 904 Salamy, K.A & Zachos, J.C. Latest Eocene-Early Oligocene climate change and Southern Ocean fertility: inferences
905 from sediment accumulation and stable isotope data. *Paleogeography, Paleoclimatology, Paleoecology*, 145, 61-77.
906 [https://doi.org/10.1016/S0031-0182\(98\)00093-5](https://doi.org/10.1016/S0031-0182(98)00093-5), 1992.
- 907 Sarkar, S., Basak, C., Frank, M. Late Eocene onset of the Proto-Antarctic Circumpolar Current. *Science Reports*, 9,
908 10125, 2019.
- 909 Sarmiento, J.L., Gruber, N., Brzezinski, M.A., Dunne, J.P. High-latitude controls of thermocline nutrients and low
910 latitude biological productivity. *Nature* 247, 56–60, 2004.
- 911 Sauermilch, I., Whittaker, J.M., Klocker, A. et al. Gateway-driven weakening of ocean gyres leads to Southern Ocean
912 cooling. *Nat Commun* 12, 6465. <https://doi.org/10.1038/s41467-021-26658-1>, 2021.
- 913 Shackleton, N.J. and Opdyke, N.D. Oxygen isotope and paleomagnetic stratigraphy of equatorial Pacific core V28-238:
914 Oxygen isotope temperatures and ice volumes on a 105 year and 106 year scale. *Quat. Res.*, 3(1), 39-55,
915 doi:10.1016/0033-5894(73)90052-5, 1973.
- 916 Shackleton, N. J., and Kennett, P. Paleotemperature history of the Cenozoic and the initiation of Antarctic glaciation:
917 Oxygen and carbon isotope analysis in DSDP Sites 277, 279 and 281, Initial Rep. Deep Sea Drill. Proj., 29, 881–884,
918 1975.
- 919 Shackleton, N.J., Hall, M.A., Boersma, A. Oxygen and carbon isotope data from Leg 74 foraminifers. *Init. Rep. Deep
920 Sea Drilling Proj.*, 74, pp. 599-612, 1984.
- 921 Scher, H.D., Martin, E.E. Circulation in the Southern Ocean during the Paleogene inferred from neodymium isotopes.
922 *Earth Planet. Sci. Lett.* 228, 391–405. <https://doi.org/10.1016/J.EPSL.2004.10.016>, 2004.
- 923 Scher, H. D. and Martin, E. E. Timing and climatic consequences of the opening of Drake Passage. *Science*, 312, 428–
924 430. DOI: 10.1126/science.1120044, 2006.
- 925 Scher, H.D., Bohaty, S.M., Smith, B.W., Munn, G.H. Isotopic interrogation of a suspected late Eocene glaciation.
926 *Paleoceanography* 29, 628–644. <https://doi.org/10.1002/2014PA002648>, 2014.
- 927 Scher, H., Whittaker, J., Williams, S. et al. Onset of Antarctic Circumpolar Current 30 million years ago as Tasmanian
928 Gateway aligned with westerlies. *Nature* 523 580–583. <https://doi.org/10.1038/nature14598>, 2015.



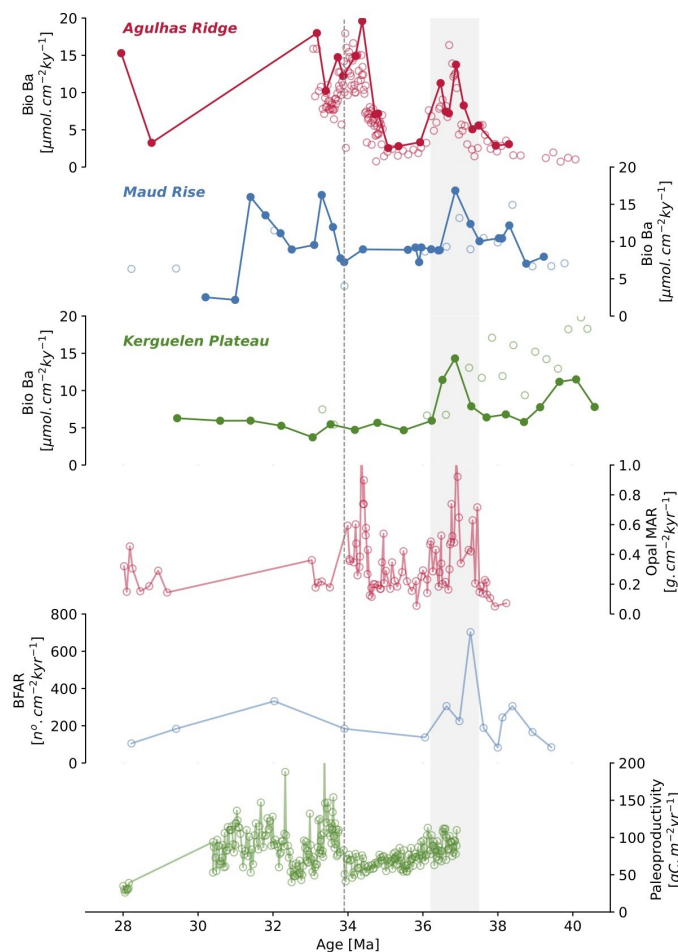
- 929 Schumacher, S. and Lazarus, D. Regional differences in pelagic productivity in the late Eocene to early Oligocene—a
930 comparison of southern high latitudes and lower latitudes. *Paleogeography, Paleoclimatology, Paleoecology*, 214, 243–
931 263. <https://doi.org/10.1016/j.palaeo.2004.06.018>, 2004.
- 932 Seton, M., Müller, R., Zahirovic, S., Gaina, C., Torsvik, T., Shephard, G., Talsma, A., Gurnis, M., Turner, M., Maus, S.,
933 and Chandler, M. Global continental and ocean basin reconstructions since 200Ma. *Earth-Science Reviews*, 113:212–
934 270. <https://doi.org/10.1016/j.earscirev.2012.03.002>, 2012.
- 935 Sijp, W. P., England, M. H. and Toggweiler, J. R. Effect of Ocean Gateway Changes under Greenhouse Warmth, *J.*
936 *Clim.*, 22(24), 6639–6652, doi:10.1175/2009JCLI3003.1, 2009.
- 937 Sijp, W. P., England, M.H., and Huber, M. Effect of the deepening of the Tasman Gateway on the global ocean.
938 *Paleoceanography*, 26, doi:10.1029/2011PA002143, 2011.
- 939 Sokolov, S., Rintoul, S.R. On the relationship between fronts of the Antarctic Circumpolar Current and surface
940 chlorophyll concentrations in the Southern Ocean. *J. Geophys. Res.* 112, 2007.
- 941 Sokolov, S. Rintoul, S.R. Circumpolar structure and distribution of the Antarctic Circumpolar Current fronts: 1. Mean
942 circumpolar paths. *J. Geophys. Res.* 114, 2009.
- 943 Spiess, V. (1990) Cenozoic magnetostratigraphy of Leg 113 drill sites, Maud Rise, Weddell Sea, Antarctica, In: Barker,
944 P. F., et al., (eds). *Proceedings of the Ocean Drilling Program: College Station, Texas, Scientific Results*, v. 113, p. 261–
945 318.
- 946 Stickley, C.E., Brinkhuis, H., Schellenberg, S.A., Sluijs, A., Röhl, U., Fuller, M., Grauert, M., Huber, M., Warnaar, J.,
947 Williams, G.L. Timing and nature of the deepening of the Tasmanian Gateway. *Paleoceanography*, 19 (4).
948 <https://doi.org/10.1029/2004PA001022>, 2004.
- 949 Taylor, V. E., Westerhold, T., Bohaty, S.M., Backman, J., Dunkley Jones, T., Edgar, K. M., Egan, K. E., Lyle, M.,
950 Pälike, H., Röhl, U., Zachos, J., Wilson, P. A. Transient Shoaling, Over-Deepening and Settling of the Calcite
951 Compensation Depth at the Eocene-Oligocene Transition. *Paleoceanography and Paloclimatology*, 38(6),
952 <https://doi.org/10.1029/2022PA004493>, 2023
- 953 Thole, L.M., Amsler, H.E., Moretti, S., Auderset, A., Gilgannon, J., Lippold, J., Vogel, H., Crosta, X., Mazaud, A.,
954 Michel, E., Martínez-García, A., Jaccard, S.L. Glacial-nterglacial dust and export production records from the Southern
955 Indian Ocean. *Earth Planet. Sci. Lett.* 525, 115716. <https://doi.org/10.1016/j.epsl.2019.115716>, 2019.
- 956 Thomas, E. Late Cretaceous through Neogene deep-sea benthic foraminifera (Maud Rise, Weddell Sea, Antarctica).
957 *Proc. Ocean Drill. Program Sci. Results* 113, 571–594, 1990.
- 958 Toggweiler, J. R. and Samuels, B. Effect of Drake Passage on the global thermohaline circulation. *Deep-Sea Res. I* 42,
959 477–500, 1995.
- 960 Toggweiler, J.R. and Bjornsohn, H. Drake Passage and paleoclimate. *Journal of Quaternary Science*, 15 (4) 319-328.
- 961 Toumoulin, A., Donnadieu, Y., Ladant, J., Batenburg, S.J., Poblete, F. and Dupont-Nivet, G. (2020). Quantifying the
962 Effect of the Drake Passage Opening on the Eocene Ocean. *Paleoceanography and Paloclimatology*, 35(8)
963 <https://doi.org/10.1029/2020PA003889>, 2000.
- 964 Van Breedam, J., Huybrechts, P., Crucifix, M. Modelling evidence for late Eocene Antarctic glaciations, *Earth and*
965 *Planetary Science Letters*, 586, 117532, ISSN 0012-821X, <https://doi.org/10.1016/j.epsl.2022.117532>, 2022.
- 966 Vonhof, H.B., Smit, J., Brinkhuis, H., Montanari, A., and Nederbragt, A.J. Global cooling accelerated by early late
967 Eocene impacts: *Geology*, v. 28, p. 687–690, doi: 10.1130/0091-7613(2000)028.3.CO;2, 2000.
- 968 Villa, G., Fiorini, C., Persico, D., Roberts, A.P. Florindo, F. Middle Eocene to Late Oligocene Antarctic
969 glaciation/deglaciation and Southern Ocean productivity. *Paleoceanography and Paloclimatology*, 29, 223-237.
970 <https://doi.org/10.1002/2013PA002518>, 2014.
- 971 Wei, W. Paleogene chronology of Southern Ocean drill holes: An update, in Kennett, J.P., and Warnke, D.A., eds., *The*
972 *Antarctic paleoenvironment: A perspective on global change: Antarctic Research Series*, v. 56, p. 75–96, 1992.
- 973 Wei, W., and Wise, S.W. Jr. Eocene-Oligocene calcareous nannofossil magnetobiochronology of the Southern Ocean:
974 *Newsletters on Stratigraphy*, v. 26, p. 119–132, 1992.
- 975 Westerhold, T., Marwan, N., Drury, A.J., Liebrand, D., Agnini, C., Anagnostou, E., Barnet, J.S.K., Bohaty, S.M.,
976 Vleeschouwer, Florindo, F., Frederichs, T., Hodell, D.A., Holbourn, A.E., Kroon, D., Laurentano, V., Littler, K., Lourens,
977 L.J., Lyle, M., Pälike, H., Röhl, U., Tian, J., Wilkens, R.H., Wilson, P.A. and Zachos, J.C. An astronomically dated
978 record of Earth’s climate and its predictability over the last 66 million years. *Science*, 369, 6509, 1383-1387. DOI:
979 10.1126/science.aba6853, 2020.
- 980 Wright, N.M., Scher, H.D., Seton, M., Huck, C.E., Duggan, B.D. No change in Southern Ocean Circulation in the
981 Indian Ocean from the Eocene through Late Oligocene. *Paleoceanography, Paleoclimatology*, 33, 152–167.
982 <https://doi.org/10.1002/2017PA003238>, 2018.
- 983 Zachos, C. J., T. M. Quinn, and K. A. Salamy. High-resolution (104 years) deep-sea foraminiferal stable isotope records
984 of the Eocene-Oligocene climate transition, *Paleoceanography*, 11, 251–266, 1996.
- 985 Zachos, C. J., B. N. Opdyke, T. M. Quinn, C. E. Jones, and A. N. Halliday. Early Cenozoic glaciation, Antarctic
986 weathering, and seawater $87\text{Sr}/86\text{Sr}$: Is there a link? *Chem. Geol.*, 161, 165–180, 1999.
- 987 Zachos, J., Pagani, M., Sloan, L., Thomas, E., Billups, K. Trends, rhythms and aberrations in global climate 65 Ma to
988 present. *Science*, 292, 686-693. <https://doi.org/10.1126/science.1059412>, 2001.



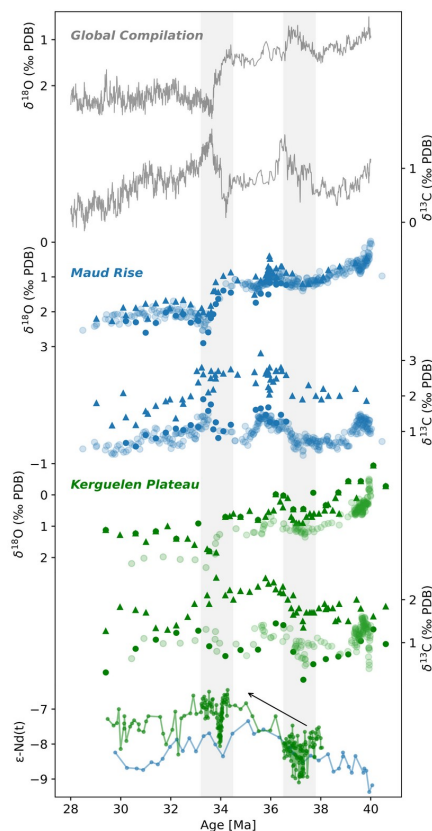
989 Zachos, J., Kump, L. Carbon cycle feedbacks and the initiation of Antarctic glaciation in the earliest Oligocene. *Global*
990 *and Planetary Change*, 47 (1). 51-66 doi:10.1016/j.gloplacha.2005.01.001, 2005.
991 Zhang, Y. G., Pagani, M., Liu, Z., Bohaty, S. M., and DeConto, R. A 40-million-year history of atmospheric CO₂.
992 *Philosophical Transactions of the Royal Society A*, v. 371, https://doi.org/10.1098/rsta.2013.0096, 2013.



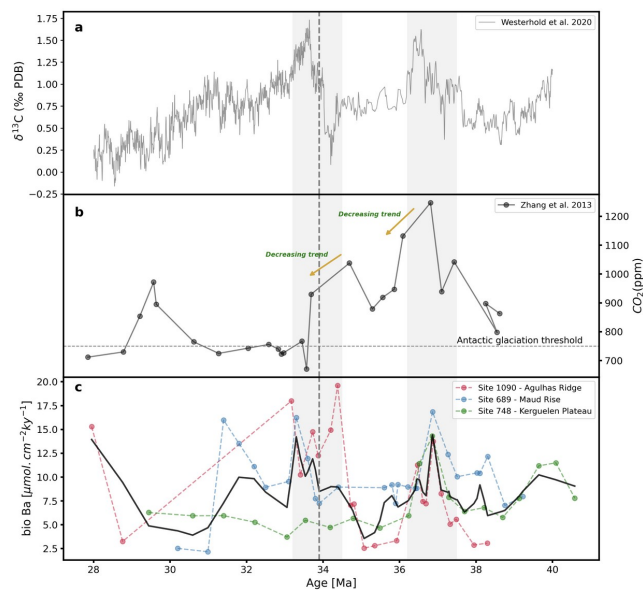
993 **Figure 1: Schematic Antarctic Circumpolar Current (ACC) and Southern Ocean fronts as determined by Orsi et**
994 **al., 1995, named from north to south, STF: Subtropical front, SAF: Subantarctic Front; PF: Polar Front and**
995 **SACCF: Southern Antarctic Circumpolar Current Front, and sBdy: Southern Boundary front. Modern location**
996 **of ODP sites (1090, Agulhas Ridge; 689, Maud Rise and 748, Kerguelen Plateau) used for reconstructions in this**
997 **study. ODP = Ocean Drilling Program.**



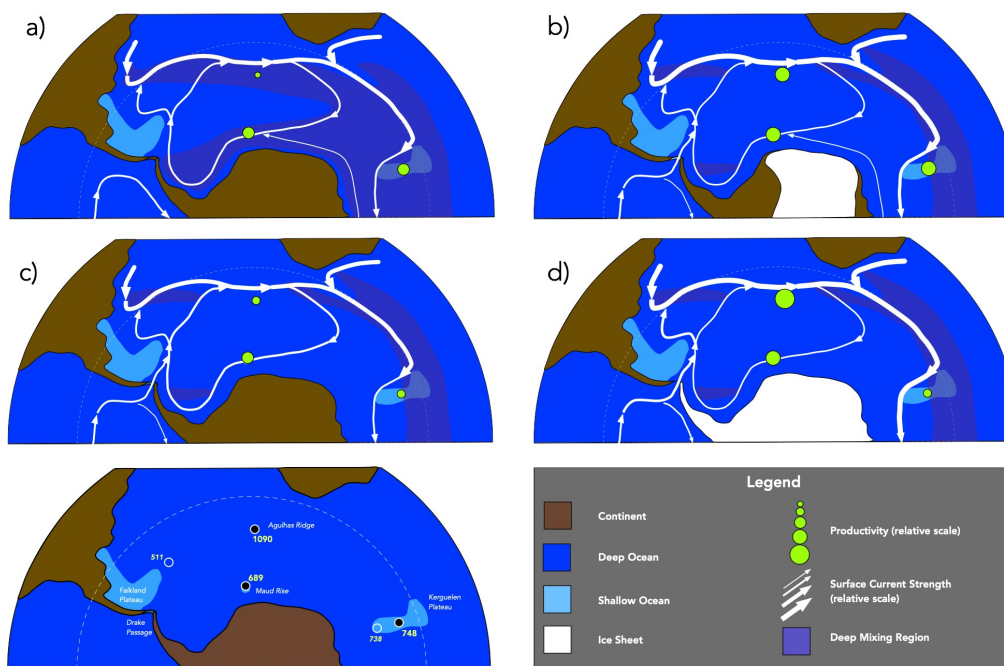
998 **Figure 2: Paleoproductivity proxies vs Age (Ma) for Agulhas Ridge (ODP Site 1090, in red), Maud Rise (ODP Site**
 999 **689, in blue) and Kerguelen Plateau (ODP Sites 748, 744 and 738, in green). Solid circles are new biogenic**
 1000 **barium accumulation rate (bio-Ba, $\mu\text{mol cm}^{-2} \text{kyr}^{-1}$) data of this study, open circles from prior literature (Agulhas**
 1001 **Ridge data from Anderson and Delaney, 2005; Maud Rise data from Diester-Haass and Faul 2019; Kerguelen**
 1002 **Plateau data from Faul et al., 2010). Site 1090 opal MAR data are from Dickmann et al., 2004. Site 689 BFAR**
 1003 **data are from Diester-Haass and Zahn 1996. Kerguelen Plateau Site 744 paleoproductivity data from Diester-**
 1004 **Haass (1996). Vertical bar identifies the E/O boundary (at ca 33.8 Ma). Shaded area encompasses the late-Eocene**
 1005 **productivity event.**



1006 **Figure 3: Multiproxy records from the late Eocene and early Oligocene. Global compilation of oxygen and**
 1007 **carbon stable isotopes (from Westerhold et al., 2020). New generated oxygen and carbon benthic foraminiferal**
 1008 **isotopes data (solid circles) and fine fraction (<45µm) (solid triangles), and previously published oxygen and**
 1009 **carbon stable isotopes (shaded circles, from Mackensen and Ehrmann, 1992; Diester-Haass and Zahn, 1996;**
 1010 **Bohaty et al., 2003) from Atlantic Southern Ocean (Maud Rise) ODP Site 689 (in blue) and Indian Southern**
 1011 **Ocean (Kerguelen Plateau) ODP Site 748 (in green). PDB is PeeDee Belemnite carbonate reference. Compilation**
 1012 **of εNd data obtained from fossil fish teeth for the Atlantic Sector of SO (Maud Rise - in blue, site 689), and for**
 1013 **the Indian sector of SO (Kerguelen Plateau - in green, sites 738 and 748) (Scher and Martin, 2004, 2006; Scher et**
 1014 **al., 2014; Wright et al. 2018). Shaded area identifies E/O boundary at ca 33.8 Ma and the changes in ocean**
 1015 **circulation. Note inverted y-axis scales for oxygen and Nd isotopes.**



1016 **Figure 4: Comparison between (a) a global compilation of carbon stable isotopes (from Westerhold et al., 2020),**
1017 **(b) alkenone-based atmospheric $p\text{CO}_2$ record (from Zhang et al., 2013) and (c) biogenic Barium (bio-Ba) export**
1018 **productivity proxy. Antarctic glaciation thresholds (approx. 750 ppm) (from climate model, DeConto et al. 2008)**
1019 **is marked by a dashed line. Shaded areas encompass the late-Eocene and early-Oligocene high productivity**
1020 **intervals.**



1021 **Figure 5: Interpretive scenario of paleoceanographic change in the late Eocene to earliest Oligocene Southern**
 1022 **Ocean. Base map, circulation patterns and extent of deep mixing regions largely after Toumoulin et al. (2020), ice**
 1023 **sheet extent at 38 Ma after models in Van Breedam (2022). Productivity values based on results of this study,**
 1024 **shown in relative scale. Note general trend towards higher productivity values, and within this, higher**
 1025 **productivity, focussed near proto-ACC, during intervals with inferred ice sheets.**